N-Glycome regulation limits the transdifferentiation of endothelial cells into hematopoietic stem cells

Authors:

Dionna M. Kasper[1, 2, 4], Yinyu Wu[1, 2, 4], Hanna K. Mandl[1, 2, 4], Kevin Salinas[1, 2, 4], Joey Ghersi[1, 2, 4], Jared Hintzen[1, 2, 4], William Armero[1, 2, 4], Zhiheng He[1, 2, 4], Daniel W. Heindel[5,6], Eon Joo Park[3, 4], William C. Sessa[3, 4], Lara K. Mahal[5,6], Karen K. Hirschi[1, 2, 4*], Stefania Nicoli[1,2,3,4*]

Affiliations:

[1]Yale Cardiovascular Research Center, Department of Internal Medicine, Section of Cardiology, Yale University School of Medicine, New Haven, CT 06511, USA [2]Department of Genetics, [3] Department of Pharmacology, Yale University School of Medicine, New Haven, CT 06510, USA, [4]Vascular Biology & Therapeutics Program, Yale University School of Medicine, New Haven, CT 06520, USA [5]Interdisciplinary Melanoma Cooperative Group, Perlmutter Cancer Center New York University School of Medicine, New York, NY 10016, USA [6]Biomedical Chemistry Institute, Department of Chemistry, New York University, New York, NY 10003, USA

*corresponding authors stefania.nicoli@yale.edu; karen.hirschi@yale.edu

Abstract:

Hematopoietic stem and progenitor cells (HSPCs) are required to establish and maintain the adult blood system in vertebrates. During development, hemogenic endothelial cells undergo an endothelial-to-hematopoietic transition (EHT) to generate HSPCs[1-4]. Growth factors and epigenetic changes can promote EHT[1,3,5], but these mechanisms do not explain its tight spatiotemporal regulation during development. Here, we show that microRNA (miR) miR-223-mediated regulation of N-glycan biosynthesis intrinsically restrains EHT, representing the first pathway that prevents excessive HSPC production. We find that miR-223 is uniquely expressed in hemogenic endothelial cells undergoing EHT and in nascent HSPCs. Loss of miR-223 promotes the expansion of these cells in the zebrafish and mouse aorta-gonad-mesonephros (AGM), where EHT occurs[6-8]. miR-223 targets *alg2* (α1,3/ α1,6 mannosyltransferase) and *st3gal2 (*α2,3 sialyltransferase) for repression in the AGM endothelium. These two enzymes are

involved in the biosynthesis of N-glycans, a common co-translational modification[9,10] that influences several pathophysiological processes[11,12], but has not yet been implicated in EHT. Using an N-glycosensor, we demonstrate that vascular N-glycosylation increases during EHT, and this process is disrupted upon loss of miR-223. Specifically, high-throughput glycome analysis revealed terminal α1,3 mannose and α2,3 sialic acid modifications of membrane proteins are altered upon loss of miR-223. Importantly, pharmacological manipulation targeting these N-glycan types in wild-type embryos phenocopies the loss of miR-223 and enhances EHT as well as HSPC production. Thus, the N-glycome plays a previously unappreciated role as an intrinsic negative regulator of EHT, with specific mannose and sialic acid modifications serving as key endothelial determinants of the hematopoietic fate.

Zebrafish endothelial-to-hematopoietic transition (EHT) has emerged as an instrumental model to understand the formation and regulation of definitive hematopoietic stem and progenitor cells (HSPCs) with long-term engraftment capability. As in their mammalian counterparts, EHT occurs in endothelial cells that co-express vascular and hematopoietic genes (hemogenic endothelial cells, hemECs). Through the progressive loss of endothelial gene expression and concomitant increase in hematopoietic potential[1-4,13], hemECs give birth to nascent HSPCs that delaminate from the vascular wall into the circulation to colonize secondary hematopoietic organs[6-8]. This process is highly regulated, involving a precise interplay between multiple developmentally-timed signaling pathways[1-5,13-16]. It is currently unclear whether such precision is achieved exclusively by the regulation of positive hematopoietic regulators, or whether yet-unknown inhibitory pathways play a role in EHT dynamics.

To discover underlying mechanisms of EHT inhibition, we investigated the function of miR-223, a miRNA enriched in zebrafish endothelial cells; genetic deletion of miR-223 results in HSPC expansion in the AGM[17]. We generated a transgenic reporter to examine miR-223 expression during EHT. Specifically, we used CRISPR/Cas9 genome editing to integrate the Gal4 transcriptional activator[18] downstream of the endogenous miR-223 promoter (miR-223:Gal4), and coupled it with a *Tg(5XUAS:eGFP)*^{nkuasgfp1a} and an endothelial cell *Tg(kdrl:hras-mCherry)*^{s896} marker. This approach fluorescently labels miR-223-expressing endothelial cells

62 with both GFP and mCherry (hereafter referred to as miR-223:GFP+ kdrl:mCH+) (Fig. 1a, b and
63 Supplementary Fig. 1a).

64 miR-223:GFP+ kdrl:mCH+ cells were dispersed in a salt and pepper pattern, with the
65 majority of cells positioned within the AGM (Fig. 1a-c). We found that the AGM population of
66 miR-223:GFP+ kdrl:mCH+ cells increased from the onset of EHT at 24 hours post fertilization
67 (hpf) to its peak at 32 hpf (Fig. 1c). In addition, they manifested a heterogeneous pattern of flat
68 to bulging morphologies, and underwent delamination from the AGM (Fig. 1a, Supplementary
69 Fig. 1b, c and Supplementary Movie 1). Importantly, miR-223:GFP+ kdrl:mCH+ cells co-
70 expressed the endothelial marker *kdrl* and hemEC markers *gata2b*[19] and *runx1*[20,21], as wells as
71 the nascent HSPC marker *cmyb*[22] (Fig. 1d), suggesting that miR-223 is expressed in hemECs
72 undergoing EHT.

73 To understand how miR-223 affects EHT, we analyzed the miR-223 mutant (miR-
74 223Δ/Δ) zebrafish AGM, and observed increased numbers of hemECs expressing *gata2b* at 24
75 hpf, as well as the downstream factor *runx1* at 27 hpf (Fig. 2a, b and Supplementary Fig. 2a,
76 b). Congruently, the kdrl:mCH+ cmyb:GFP+ nascent HSPC population[6] was enlarged for the
77 duration of EHT (Fig. 2a, c and Supplementary Fig. 2c), resulting in HSPC overexpansion at
78 subsequent hematopoietic sites[17]. Importantly, expression of the wild-type miR-223 gene in miR-
79 223:Gal4+ or in endothelial *fli1a+* cells rescued the HSPC overexpansion in miR-
80 223Δ/Δ zebrafish (Supplementary Fig. 2d-g), verifying that miR-223 functions in endothelial
81 cells of the AGM to limit HSPC production. Taken together, these findings support that miR-223
82 intrinsically restricts EHT in hemECs.

83 To further corroborate miR-223 function, we analyzed hemEC and HSPC populations
84 during mammalian EHT. We observed abundant miR-223 expression in sorted mouse hemECs
85 (Flk+cKit+CD45-SP+)[23] and endothelial cells (CD31+CD45-SP-) relative to non-endothelial
86 cells isolated from the embryonic day (e) 10.5 AGM, the primary site of definitive HSPC
87 production[2,7] (Fig. 2d, e). Mice with a global miR-223 knockout (KO)[24] displayed elevated
88 hemECs in the e10.5 AGM compared to wild-type (Fig. 2f). Subsequently, HSPCs (cKit+Sca+
89 Lin-) were expanded in miR-223 KO mice at secondary hematopoietic sites, namely the fetal
90 liver at e14.5 and the fetal bone marrow at e18.5 (Fig. 2d, f). These results establish miR-223 as
91 a conserved endothelial inhibitor of HSPC production.

92 Next, we sought to identify the miR-223-dependent mechanism limiting EHT in hemECs.
93 miRNAs can fine tune gene expression by targeting mRNAs for decay, typically via
94 complementary base-pairing to sites within 3' untranslated regions (3' UTRs), known as miRNA
95 responsive elements (MREs)[25,26]. Therefore, we performed comparative mRNA profiling of
96 zebrafish wild-type and miR-223Δ/Δ endothelial cells at the start of EHT[17], and validated the
97 results by qRT-PCR (Fig. 3a). Amongst the top transcripts most upregulated upon loss of miR-
98 223 and harboring a predicted miR-223 MRE were genes involved in generating N-glycosylated
99 proteins (Fig. 3a, b and Supplementary Fig. 3a).
100 N-glycosylation involves the co-translational attachment and processing of
101 oligosaccharides (glycans) onto asparagine (N) residues of secreted or membrane-bound proteins
102 and regulates protein folding, stability, and activity[9,10] (Fig. 3b and Supplementary Fig. 3a). N-
103 glycosylation begins in the endoplasmic reticulum (ER), where a preassembled dolichol lipid-
104 linked sugar glycan core is transferred *en bloc* onto nascent polypeptide chains. The N-glycan is
105 then progressively processed in the ER and Golgi apparatus as the protein traffics to the cell
106 membrane. The putative miR-223 target *alg2* is an ER mannosyltransferase involved in adding α
107 1,3 / α 1,6-linked mannose moieties to the N-glycan core[9,27]. Mannose-binding lectin *lman2lb*,
108 another candidate miR-223 target, promotes N-glycoprotein transport from the ER to the Golgi
109 apparatus[28,29]. The putative miR-223 target *st3gal2*, is a sialyltransferase that adds α 2,3-linked
110 sialic acid sugars to the N-glycan in the Golgi apparatus[30-32] (Fig. 3b and Supplementary Fig. 3a).
111 To determine whether miR-223 binds and regulates these three transcripts during EHT,
112 we developed sensors[33] of miR-223 activity consisting of mCherry fused to a short *alg2*, *lman2lb*,
113 or *st3gal2* 3'UTR fragment that contains the putative miR-223 MRE (Supplementary Fig. 3b).
114 Expression of both the mCherry sensor and an eGFP that lacks a 3'UTR (for normalization) was
115 driven from a bidirectional and endothelial-specific *fli1a* promoter. We injected these constructs
116 into wild-type, miR-223Δ/+ and miR-223Δ/Δ zebrafish embryos and observed mCherry and
117 eGFP expression in endothelial cells, as expected. Importantly, the mCherry:eGFP ratios from
118 the *alg2* and *st3gal2* sensors were significantly higher in individual AGM endothelial cells in to
119 in miR-223Δ/+ and miR-223Δ/Δ embryos compared to wild-type embryos during the peak of
120 EHT at 32 hpf (Supplementary Fig. 3c-g). These data suggest that miR-223 directly binds and
121 represses *alg2* and *st3gal2* transcripts in AGM endothelial cells. In contrast, the mCherry:eGFP

122 ratio from the *lman2lb* sensor was similar in individual AGM endothelial cells from wild-type
123 and mutant embryos, suggesting indirect regulation.

124 We generated a stable line of the *alg2* 3'UTR-miR-223 sensor for mutational analysis of
125 the MRE. CRISPR/Cas9-mediated mutation of the MRE led to an increased mCherry:eGFP ratio
126 in the AGM (Fig. 3c, d and Supplementary Fig. 3h), consistent with de-repression in miR-
127 223Δ/Δ . Further, mutation of the endogenous miR-223 MRE within the *alg2* 3'UTR
128 phenocopied the HSPC overexpansion observed in miR-223Δ/Δ zebrafish, both in the 32 hpf
129 AGM and the 54 hpf caudal hematopoietic tissue[34] (the hematopoietic site analogous to the
130 mammalian fetal liver) (Fig. 3e-g). Thus, these data suggest that miR-223 directly inhibits *alg2*
131 and/or *st3gal2* to limit HSPC production at the site of EHT, potentially via altered N-
132 glycosylation.

133 To investigate whether N-glycosylation changes during EHT, we generated an N-
134 glycosylation reporter. The reporter contains an N-glycosensor[35], consisting of firefly luciferase
135 fused to an ER translation sequence. ER translocation of firefly luciferase results in its N-
136 glycosylation and reduced bioluminescence[35] (Fig. 4a). The reporter also contains a renilla
137 luciferase (for normalization), and both genes are driven by the *fli1a* promoter (Fig. 4a).
138 Injection of the endothelial-specific N-glycosylation reporter into wild-type embryos revealed a
139 decrease in firefly luminescence from 24 hpf to 32 hpf, indicating that endothelial cell N-
140 glycosylation naturally increased from the onset to the peak of EHT (Fig. 4b). In addition, miR-
141 223Δ/Δ embryos showed increased firefly luminescence at 32 hpf compared to controls (Fig. 4c),
142 consistent with defective N-glycosylation of firefly luciferase upon dysregulation of miR-223.
143 Thus, N-glycosylation is regulated by miR-223 during EHT.

144 The increased luminescence of the N-glycosensor upon loss of miR-223 function could
145 reflect reduced N-glycan addition or altered N-glycan processing. To distinguish between these
146 possibilities, we first tested whether blocking N-glycan addition recapitulates HSPC
147 overexpansion in miR-223Δ/Δ embryos. We treated wild-type zebrafish during EHT with
148 tunicamycin (TM), an N-acetylglucosamine (GlcNAc)-1-phosphotransferase inhibitor that
149 prevents N-glycan core attachment to nascent polypeptides, leading to protein misfolding and ER
150 stress[36,37]. TM treatment increased firefly luminescence as expected[35], but did not result in an
151 overexpansion of *cmyb*+ HSPCs at 32 hpf (Supplementary Fig. 4a, b). Likewise, *cmyb*+
152 expression did not increase upon treatment with thapsigargin, an N-glycosylation-independent

153 inducer of ER-stress[36] (Supplementary Fig. 4c). Thus, miR-223Δ/Δ hematopoietic defects do not
154 arise from an overall reduction in protein N-glycosylation or general ER stress.

155 To investigate whether N-glycan processing is disrupted by loss of miR-223, we used a
156 ratiometric lectin microarray strategy to analyze the glycomes of wild-type and mutant zebrafish
157 embryos[38]. We isolated membrane proteins from 32 hpf wild-type and miR-223Δ/Δ embryos,
158 and deciphered differences in specific sugar modifications based on their differential binding to
159 over 90 lectins or antibodies on the array[39]. Notably, glycoproteins from miR-223Δ/Δ embryos
160 had significantly increased levels of terminal α1,3-linked mannose modifications, as well as
161 decreased levels of α2,3-linked sialic acid and bisecting GlcNAc, compared to those from wild-
162 type (Fig. 4d, e). Thus, loss of miR-223 affects N-glycan processing.

163 Next, we determined whether compounds that alter N-glycan processing could promote
164 EHT and HSPC overexpansion, similar to loss of miR-223. Briefly, we treated wild-type
165 embryos undergoing EHT with swainsonine (SW) to enhance mannose-biased modification[37], or
166 a pan-sialyltransferase inhibitor (ST) to diminish terminal sialic acid incorporation[40] (Fig. 4 f-j
167 and Supplementary Fig. 4d). Remarkably, both SW and ST treatments of wild-type embryos
168 resulted in the overexpansion of kdrl:mCH+ cmyb:GFP+ cells and *cmyb*+ nascent HSPCs in the
169 AGM at 32 hpf, recapitulating the miR-223Δ/Δ phenotype (Fig. 2c, Fig. 4g, h, j, and
170 Supplementary Fig. 4d). Taken together, we find that a distinct N-glycome established by miR-
171 223 limits the production of HSPCs from hemECs (Fig. 4k).

172 In summary, our data reveal an unanticipated role for the N-glycan biosynthesis pathway
173 in limiting HSPC production during EHT, thus illuminating how this process occurs. We found
174 that hemECs in the AGM possess an intrinsic mechanism to restrict EHT based on a "sugar
175 code", comprised of a specific level of cell surface glycans, α1,3 mannose and α2,3 sialic acid.
176 This regulation is mediated by miR-223-dependent repression of N-glycan biosynthesis genes,
177 which regulates the glycan repertoire (Fig. 4k).

178 Importantly, these findings lay the foundation for future mechanistic studies on how the
179 diverse array of hematopoietic regulators are limited in their activity by a common co-
180 translational modification, protein N-glycosylation. The discovery that EHT is regulated by a
181 specific glycan profile presents new exciting avenues for regulating *in vivo* and *ex-vivo* blood
182 stem cell production[41,42]. The wide variety of glycan metabolism modifiers and inhibitors could
183 be used to glyco-engineer cells, optimizing the production of glycoforms that facilitate the

184 reprogramming of somatic cells to HSPCs[43-45]. Thus, the application of our knowledge and
185 approaches could significantly improve HSPC production for therapeutic interventions of blood
186 disorders.
187
188 **Methods**
189 **Animal Strains and Husbandry**
190 Zebrafish were raised and maintained at 28.5˚C using standard methods (unless otherwise
191 indicated), and according to protocols approved by Yale University Institutional Animal Care
192 and Use Committee (# 2017-11473). AB was used as the wild type genetic background.
193 Zebrafish transgenic strains generated in this study are: *Tg(miR-223:KalTA4)*^{ya362}(wt
194 background)*; Tg(miR-223:KalTA4)*^{ya363} (miR-223^{ya303} background)*, Tg(fli1ep:mCherry-alg2*
195 *3'UTR sensor: eGFP)*^{ya364} (referred to as *alg2* 3'UTR-miR-223 MRE sensor). The following
196 lines have been described previously: miR-223^{ya303} and miR-223^{ya304} (referred to as miR-
197 223Δ/Δ)[17], *Tg(kdrl:gfp)*^{la116} (referred to as kdrl:GFP+)[46], *Tg(gata2b:KalTA4)*^{sd32} coupled with
198 *Tg(UAS:lifeact-GFP)*^{mu271} (referred to as gata2b:GFP+)[19]*; Tg(kdrl:hras-mCherry)*^{s896} (referred to
199 as kdrl:mCH)[6]; *Tg(kdrl:mCherry)*^{is5} *Tg(cmyb:GFP)*^{zf169} (referred to as kdrl:mcH+cmyb:GFP+)[6],
200 *Tg(5xUAS:eGFP)*^{nkuasgfp1a} (referred to as UAS:GFP)[47]. For clarity, *Tg(miR-223:kalTA4)* is
201 referred to as miR-223:Gal4+ or when coupled with *Tg(5xUAS:eGFP)*^{nkuasgfp1a} is called miR-
202 223:GFP+. Zebrafish embryos and adults were genotyped as described[17]. See Table 1 for
203 genotyping primers.
204 All mouse experiments were approved by Yale University Institutional Animal Care and
205 Use Committee (#2017-11447). Mouse stains used in this study were wild-type (Jackson
206 #002014) and miR-223KO (Jackson #013198) in the C57BL/6 background. Mouse embryos
207 were generated from timed matings between females and males (>8 weeks). The morning of
208 detection of vaginal plug was defined as e0.5.
209
210 **Generation of miR-223:Gal4 reporter zebrafish**
211 To generate the miR-223:Gal4 reporter line, the improved Gal4 variant KalTA4[48] was inserted
212 into the endogenous miR-223^{+} (wild-type) or miR-223^{ya303} genomic locus on Chromosome 5
213 using CRISPR/Cas9 genomic editing according to published protocols with the following
214 modifications[18]. The KalTA4 integration site was designed approximately 50 bp upstream of the

miR-223 precursor stem loop genomic sequence (miRBase Accession # MI0001389). A ~300 bp fragment surrounding this site was PCR amplified with flanking BamHI restriction sites and cloned into the eGFP bait-E2A-KalTA4-pA plasmid[49] by T4 ligation according to the manufacturer's protocols (NEB), to produce the miR-223-E2A-KalTA4 bait plasmid. CRISPRScan[50,51] was then used to design a guide RNA (gRNA) that targets both the miR-223 genomic locus and miR-223-E2A-KalTA4 bait plasmid. The gRNA template for in vitro transcription was PCR amplified and purified with Qiaquick PCR purification Kit (Qiagen). In vitro transcription followed and was performed as described[52]. High gRNA targeting efficiency at the miR-223 locus was confirmed by T7 endonuclease I (T7E1) in individual AB embryos injected with 60 pg of miR-223 gRNA and 200 pg of Cas9 mRNA as before[52]. See Table 1 for cloning and gRNA PCR primers.

To establish the stable miR-223:Gal4 reporter lines, *Tg(5xUAS:eGFP)*^{nkuasgfp1a} transgenic embryos were injected in the one-cell with 30 pg of miR-223-E2A-KalTA4 bait plasmid, 60 pg of miR-223 gRNA, 200 pg of Cas9 mRNA. Injected embryos with eGFP fluorescent cells were raised to adult hood and then outcrossed to establish the wildtype F1 founder *Tg(miR-223:KalTA4)*^{ya362}. F1 founders were then established in the *Tg(kdrl:hras-mCherry)*^{s896} background. The miR-223 mutant founder *Tg(miR-223:KalTA4)*^{ya363} was independently generated in a similar fashion except embryos from *Tg(5xUAS:eGFP)*^{nkuasgfp1a} and miR-223^{ya303} outcrosses were injected, and the KalTA4 integration on the mutant allele was confirmed.

Quantitative RT-PCR

Embryos were disassociated into single cell suspensions and subjected to Fluorescence Activated Cell Sorting (FACS) as described for transgenic zebrafish previously[53] or for mice below. 300-500 ng of total RNA isolated from the indicated FAC-sorted populations was used in miRNA or mRNA reverse transcription reactions and the resulting cDNA was used as template for SYBR Green-based quantitative PCR as before[17]. qRT-PCR primers are listed in Table 1. U6 primers (RNU6B, Hs_RNU6-2_1) were commercially provided from Qiagen.

The $2^{-\Delta\Delta CT}$ method was used to determine relative gene expression for quantitative RT-PCR analyses. Mature miRNA expression was normalized to U6 snRNA levels and was relative to the indicated control. mRNA levels were normalized to the beta actin housekeeping

245 gene, *actb1* and was relative to the indicated control. Statistical comparisons between replicate
246 pair ΔCT values for indicated groups were determined by a paired, two-tailed Student's t-test.
247
248 **Immunofluorescence**
249 Immunofluorescence was performed as follows to amplify GFP and mCherry expression in
250 zebrafish embryos imaged by confocal microscopy unless otherwise indicated. After overnight
251 4% formaldehyde fixation at 4˚C, 24, 27, 32, or 48 hpf embryos were washed with 1XPBS-
252 0.01%Tween-20 (PBSTw) 4 times for 5 minutes, and then permeabilized with 0.125% trypsin
253 (Millipore Sigma T4549) for 1, 3, 5, or 10 minutes, respectively. Embryos were washed in
254 blocking solution (0.8% Triton-X, 10% normal goat serum, 1% BSA, 0.01% sodium azide in
255 PBSTw) 3 times for 5 minutes, plus an additional 2-hour incubation with shaking. Antibody
256 concentrations used were 1:300 chicken anti-GFP (Abcam, ab13970) or rabbit anti-RFP
257 (Anitbodies Online, ABIN129578) primary antibodies and 1:400 Alexa Fluor 488 goat anti–
258 chicken IgG or Alexa Fluor 546 donkey anti-rabbit IgG (ThermoFisher) secondary antibodies.
259 Following each overnight antibody incubation at 4˚C, six washes for a total of 4 hours were
260 performed with blocking solution lacking goat serum at room temperature.
261 Immunofluorescent confocal micrographs were blinded and quantified for miR-
262 223:GFP+ kdrl:mCH+, kdrl:mCH+ gata2b:GFP, or kdrl:mCH+ cmyb:GFP cell numbers or *alg2*
263 3'UTR-miR223 MRE sensor expression (see below). Datasets that were normally distributed as
264 determined by the Shapiro-Wilk normality test were statistically evaluated by a Student's T-test;
265 otherwise, a non-parametric Mann-Whitney U test was applied.
266
267 **Whole mount in situ hybridization**
268 Whole mount in situ hybridization (WISH) was performed as previously described[17] using
269 hybridization probes for *gata2b*[19], *runx1*[54], and *cmyb*[55]. *gata2b* and *runx1* WISH staining was
270 quantified from equally-exposed, color-inverted bright field images with Image J as follows. The
271 Polygon Selection tool was used to outline the area of WISH staining along the entire length of
272 the yolk extension, corresponding to the AGM region. The mean WISH signal for the selected
273 area was obtained using the Measure tool and subtracted for mean background staining, which
274 was measured for the same area, but in a region of the trunk just above (dorsal) the AGM, which
275 lacks *gata2b* or *runx1* expression. Measurements from 2 biological replicates per genotype were

276 combined and an unpaired, two-tailed Student's t-test was applied to detect statistical differences
277 between conditions.
278 Images of *cmyb* WISH staining in the 32 hpf AGM and 54 hpf CHT for at least 12
279 embryos per replicate were blinded and then were categorized as having continuous (high) or
280 no/intermittent (low/medium) *cmyb* expression in the AGM region along the yolk extension.
281 Data was expressed as the percentage of embryos having high or low/medium staining,
282 respectively. Statistical differences between wild-type and miR-223Δ/Δ replicate pairs (collected
283 and stained on the same days) were determined by a paired, two-tailed Student's t-test.
284
285 **Flow Cytometry in Mice**
286 Mouse embryo dissection, cell isolation and flow cytometry of E10.5 AGM were performed as
287 previously described [56]. Briefly, developmental stage-matched miR-223KO and wild-type e10.5
288 AGM regions were freshly dissected and digested in 2mg/mL collagenase type II at 37 °C for
289 20 min in HBSS (Gibco) with 10% FBS (Gibco or Gemini) to obtain single-cell suspensions.
290 Cells were resuspended in DMEM (Gibco) with 10% FBS to a concentration of 2 x 10^6 cells/ml,
291 and incubated for 1 hour in 5 µg/mL Hoechst 33342 (Sigma) at 37 °C, followed by staining of
292 the following antibodies: CD45 (FITC, eBioscience 11-0451-85), c-Kit(APC, BD 553356),
293 Flk1(PE-Cy7, BD 561259), CD31 (PE, BD 553373). Single cell suspensions of e14.5 fetal liver
294 and e18.5 fetal bone marrow were immunostained with the following antibodies: c-Kit (PE,
295 eBioscience 12-1172-82), Sca-1 (FITC, eBioscience 11-5981-82), lineage antibody cocktail
296 (PerCP-Cy5.5, BD 561317). Cells were analyzed or sorted by flow cytometer LSRII or Aria (BD
297 Bioscience) respectively and flow cytometry data were analyzed with FlowJo software. Student's
298 t-test (unpaired, two tailed) was used to compare miR-223KO and wild-type relative cell
299 abundance, and data was charted as fold change relative to wild-type.
300
301 **miR-223 expression constructs**
302 miR-223 expression constructs (Supplementary Fig. 2) were constructed as previously described
303 with the following modifications[33]. To generate the pME-miR-223 middle entry cassette for
304 Gateway-compatible cloning, a 365 bp genomic sequence containing the miR-223 stem loop
305 precursor was PCR amplified with flanking KpnI and StuI sites (see Table 1), and the resulting
306 fragment was restriction digested and cloned into pME-miR using T4 ligation (NEB) according

307 to the manufacturer's protocol. Promoter entry cassettes p5E-*uasE1b* or p5E-*fli1a*[57] (Addgene
308 26026 and 31160) were utilized in LR multisite Gateway cloning reactions as before[33] to produce
309 UAS-mCherry-miR-223 and *fli1a*-mCherry-miR-223 constructs, respectively. Embryos were
310 injected in the one-cell with 25 pg each of either expression construct and Tol2 transposase
311 mRNA, and later selected for mCherry expression.
312
313 **Endothelial miR-223 sensor assays & zebrafish generation**
314 Endothelial N-glycogene 3'UTR-miR-223 MRE sensors were constructed as previously
315 described except the p3E entry vector was generated by subcloning a short (~88-117 bp) PCR
316 fragment of the *alg2*, *lman2lb*, or *st3gal2* 3'UTR that contains the miR-223 responsive element
317 using flanking SnaBI and SpeI restriction sites[33]. See Table 1 for N-glycogene 3'UTR cloning
318 primers. Mosaic expression of each sensor (Supplementary Fig. 3c, e-g) was achieved by
319 injecting single-cell embryos from miR-223Δ/+ in-crosses with 25 pg each of the sensor
320 construct and Tol2 transposase mRNA. For each expression construct, live injected embryos
321 were confocal imaged at ~32hpf using a constant exposure setting and then genotyped. Using
322 ImageJ on genotype-blinded maximum confocal projections, individual AGM endothelial cells
323 were first outlined using the Polygon Selection tool. Mean mCherry and eGFP intensities were
324 then quantified for the selected area using the Measure tool and were subtracted for mean image
325 background fluorescence in their respective channel. mCherry relative to eGFP intensities were
326 assessed for each genotype. Outlier values were removed using the ROUT method (Q= 1%) in
327 Graphpad Prism7. A Mann-Whitney U test was used for statistical comparisons.
328 To establish the stably-transmitting *Tg(fli1a:mCherry-alg2 3'UTR sensor: eGFP)*^{ya364}
329 line (Fig. 3c), embryos injected with 25 pg eaph of Tol2 transposase and *alg2* 3'UTR-miR-223
330 MRE sensor construct were raised to adulthood and an F1 founder was the crossed into both
331 wild-type and miR-223Δ/Δ backgrounds. Sensor expression was quantified with Image J as
332 described above for 32 hpf fixed and immunostained embryos, except the Segmented Line tool
333 was used to measure mCherry and eGFP intensities along length of the dorsal aorta or posterior
334 cardinal vein vessel walls above the yolk extension. An unpaired, two-tailed Student's test was
335 used for statistical comparisons.
336
337 ***alg2* 3'UTR gRNA generation & injection**

338 CRISPRScan[50,51] was used to design two gRNAs to mutate the miR-223 responsive element
339 region in the *alg2* 3'UTR with CRISPR/Cas9 genome editing. gRNA preparation was performed
340 as above for miR-223:Gal4 zebrafish generation. gRNA templates were combined prior to in
341 vitro transcription. F0 embryos injected with 100 pg of the *alg2* 3'UTR gRNA mix and 200 pg of
342 Cas9 mRNA at the one-cell stage were used to confirm mutagenesis via T7 endonuclease I
343 (T7E1) assay and sequencing as described[52] or analyzed in phenotypic assays.
344
345 **Endothelial N-glycosensor assays**
346 The previously published firefly luciferase N-glycosensor[35] was modified to allow for its co-
347 expression with a renilla luciferase normalization control as follows. The DNA fragment
348 containing the EGFR ER translation sequence and Firefly luciferase gene with three N-
349 glycosylation sites was subcloned from the pcDNA3-ERlucT vector[35] into multiple cloning site
350 (MCS) A of the pIRESneo vector (Clontech) using NotI and BamHI sites. The resulting plasmid
351 was further modified by replacing the Neomycin resistant gene, located downstream of MCS A
352 and the internal ribosome entry site (IRES), with the Renilla luciferase gene from the pRL-CMV
353 vector (Promega) using SmaI and XbaI sites. The ERlucT-IRES-Rluc bicistronic expression
354 cassette was then PCR amplified using primers listed in Table 1 and then subcloned using the
355 pCR8/GW/TOPO TA Cloning Kit (Invitrogen), to produce the Gateway cloning-compatible
356 ERlucT-IRES-Rluc-pCR8 middle entry vector. To generate the endothelial N-glycosensor
357 expression construct, Gateway entry vectors p5E-*fli1a*[57] (Addgene 31160), ERlucT-IRES-Rluc-
358 pCR8, and p3E-793[33], were recombined into destination vector pDestTol2pA[58] using LR
359 Clonase II Multisite Gateway cloning (Invitrogen) according to the manufacturer's instructions.
360 For endothelial N-glycosensor assays, embryos were injected with 25 pg each of the
361 *Tg(fli1a:ERlucT-IRES-Rluc:pDestTol2A)* construct and Tol2 transposase into the one-cell and
362 grown to the indicated developmental stages. A Dual Luciferase Reporter Assay (Promega) was
363 then performed according to manufacturer's guidelines. Briefly, 25 dechorionated embryos per
364 condition were washed once with Dulbecco's PBS (Gibco) and then incubated shaking at 200
365 rpm in 25 µl of the provided 1X Passive Lysis Buffer for 30 minutes. Embryo extracts were
366 homogenized with a pellet pestle and spun at 13,000 rpm to remove cellular debris. Firefly and
367 Renilla bioluminescence readings were obtained from 20 µl of cleared lysate using the Synergy 2
368 plate reader and Gen 5 analysis software system (BioTek). Firefly bioluminescence was

369 normalized to renilla levels, and expressed as a fold change relative to indicated control.
370 Statistical differences of normalized firefly bioluminescence values between biological replicate
371 pairs were determined by a paired, two-tailed Student's t-test.
372
373 **Lectin Microarray Glycomic Analysis**
374 Lectin microarrays were prepared as previously described[39]. Slides were generated in the Mahal
375 laboratory using Nano-plotter v2.0 piezoelectric non-contact array printer (GeSiM) with a nano
376 A-J tip to print each lectin or antibody. Arrays were printed on Nexterion Slide H (Schott
377 Nexterion) under 50% relative humidity at a surface temperature of 12°C with lectins and
378 antibodies that were purchased from Vector Labs, R&D Systems, Santa Cruz, TCI, AbCam, E.Y.
379 Labs, or Sigma-Aldrich on the array. The recombinant lectins rGRFT, rCVN, and rSVN were
380 generous gifts from Dr. B. O'Keefe (NCI Frederick). SLBR-N, SLBR-H, and SLBR-B[59] were
381 gifts from Dr. B. Bensing (UCSF).
382 Membrane protein extracts applied to the array were isolated from 32 hpf wild-type and
383 miR-223Δ/Δ zebrafish embryos and fluorescently labeled as follows. 400 dechorionated embryos
384 per replicate sample were washed two times in deyolking buffer (55mM NaCl, 1.8mM KCl,
385 1.25mM $NaHCO_3$)[60]. The yolk was separated from embryos by gentle pipetting in 250-500 µl of
386 deyolking buffer, followed by 5 minutes of room temperature shaking at 850 rpm. Samples were
387 spun at 300 rcf for 30 seconds and the yolk-containing supernatant was discarded. To remove
388 any remaining yolk, the pelleted tissue was washed with Dulbecco's PBS (Gibco), and shook at
389 850 rpm for 2 minutes for a total of two times. After a 300g, 5 minute spin at 4˚C, nearly all
390 supernatant was removed and tissue was incubated in 1 ml of cold hypotonic PBS solution
391 (10mM Na_2HPO_4, 1.8mM KH_2PO_4, 10mM KCl, 0.2mM $MgCl_2$) plus 1:100 protease inhibitor
392 cocktail set III (Millipore Sigma) for 10 minutes on ice to lyse cells. Samples were dounce-
393 homogenized 150 times with the B pestle on ice, and then spun at 500g for 5' at 4˚C to remove
394 cell debris. Protein lysates were frozen with liquid nitrogen and stored at -80˚C until used. To
395 obtain the membrane protein fraction, thawed lysates were spun at 100 kg for 1 hour at 4˚C and
396 pellets were resuspended immediately in 100 µl of cold PBS (0.1M Na_2HPO_4, 0.15M NaCl, pH
397 7.2-7.4) with 1:100 protease inhibitors. Samples were fully homogenized by passing the sample
398 through a 25G needle 10-15 times on ice.

399 Protein concentrations for individual samples were determined using a BCA protein
400 assay following the manufacturer's protocol (Thermo Scientific Pierce). 50 µg of protein were
401 labeled with Alexa Fluor 555 and all reactions were quenched using 2M Tris (pH 6.8) with no
402 further dialysis. A mixed reference was prepared following the same protocol, but labeled with
403 Alexa Fluor 647. Samples for the array were prepared by mixing 5 µg of protein from each
404 individual sample with 5 µg of the mixed reference in 0.005% PBS-Tween (pH 7.4).
405 Prior to sample hybridization, the lectin microarray slides were blocked for an hour with
406 50 mM ethanolamine in 50 mM sodium borate buffer (pH 8.8) at room temperature. They were
407 then washed 3 times with 0.005% PBS-Tween (pH 7.4). Hybridization cassettes (Arrayit) were
408 utilized to isolate individual arrays on each slide (24 per slide) and prevent leakage from one
409 sample to the next. Samples were applied to individual arrays and one array per slide was
410 reserved for a reference vs reference. Samples were incubated on the array for 2 hours at 25 °C
411 with gentle agitation. After hybridization, the samples were carefully removed and the arrays
412 were washed 4 times with 0.005% PBS-Tween (pH 7.4) for 5 minutes followed by a final wash
413 with ddH2O. The arrays were scanned using a GenePix 4300A array scanner.
414 Background-subtracted median fluorescence intensities were extracted using GenePix Pro
415 v7.2. Lectins that did not meet signal to noise ratios <2 in >90% were removed from the data
416 prior to analysis. The data was then median-normalized for each dye used and the log2 of the
417 sample/reference ratio was determined for each technical replicate. The replicates were then
418 averaged for each lectin within each array. The log2 values were then used for statistical
419 analysis (Student's T-Test) and comparison of the sample types.
420
421 **Pharmacological inhibitor treatments**
422 Zebrafish embryos were exposed to chemical inhibitors of N-glycosylation at the following
423 concentrations, 0.75 µg/ml of tunicamycin (Millipore Sigma T7765), 5 µg/ml of swainsonine
424 (Millipore Sigma S9263), 200 µg/ml of 3Fax-Peracetyl Neu5Ac Sialyltransferase Inhibitor
425 (Millipore Sigma 566224); or to 0.4 µM of thapsigargin (Millipore Sigma 586006), an N-
426 glycosylation-independent inducer of ER stress. Equal concentrations of the DMSO vehicle were
427 applied as controls for each drug as indicated. All treatments were administered from 8-32 hpf in
428 standard embryo medium with 0.003% 1-phenyl-2-thiourea (PTU) to prevent pigmentation for
429 downstream analyses.

430

431 **Image Acquisition**

432 Zebrafish embryos imaged by confocal or bright-field microscopy were raised in 0.003% PTU
433 starting after the gastrulation stage to prevent pigmentation. Embryos imaged live by confocal
434 microscopy were anesthetized in 0.1% tricaine and mounted in 1% low melt agarose. The
435 majority of fluorescent images and timelapse movie were captured using an upright Leica
436 Microsystems SP5 confocal microscope using a 25X objective except for images in Fig. 3c of the
437 stable *alg2* 3'UTR-miR-223 MRE sensor line, which were captured with an upright Leica
438 Microsystems SP8 confocal microscope. Bright field images of whole mount in situ staining
439 were acquired with a Leica Microsystems M165FC stereomicroscope equipped with Leica
440 DFC295 camera.

441
442
443 **Table 1: Primers used in this study**

Primer Name	F/R	Primer Sequence (5'-3')	Assay	Ref
dre-miR-223 gRNA	F	taatacgactcactataggcacctggctcaacatgtcgtttt agagctagaa	gRNA PCR	this study
dre-miR-223 bait BamHI	F	ggccggatccccaaggaacccaatgaactg	miR-223 Gal4 bait cloning	this study
dre-miR-223 bait BamHI	R	ggccggatccctccctcttcctcctgcttt	miR-223 Gal4 bait cloning	this study
dre-miR-223	F	tgtcagtttgtcaaatacccc	qPCR	[17]
dre-*actb1*	F	gatctggcatcacaccttctac	qPCR	[17]
dre-*actb1*	R	tcttctctctgttggctttgg	qPCR	[17]
dre-*kdrl/flk1*	F	cgaacgtgaagtgacatacgg	qPCR	[16]
dre-*kdrl/flk1*	R	ccctctaccaaaccatgtgaaa	qPCR	[16]
dre-*gata2b*	F	accaccacactctggagac	qPCR	[19]
dre-*gata2b*	R	ctgttgcgtgtctgaatacc	qPCR	[19]
dre-*runx1*	F	cgtcttcacaaaccctcctcaa	qPCR	[16]
dre-*runx1*	R	gctttactgcttcatccggct	qPCR	[16]
dre-*cmyb*	F	tgctatccagagacactacagc	qPCR	[17]
dre-*cmyb*	R	agtgcctgttgtcccttcag	qPCR	[17]
dre-*alg2*	F	gcttacctgcgcatgatctac	qPCR	this study
dre-*alg2*	R	atacaggcgcttcagagcag	qPCR	this study
dre-*lman2lb*	F	agtggaacgcagtcctgaag	qPCR	this study
dre-*lman2lb*	R	tgatgctccttccttcatcc	qPCR	this study
dre-*st3gal2*	F	ctggtgggtgatgttgcag	qPCR	this study
dre-*st3gal2*	R	cacgaaccgtatggggaac	qPCR	this study
dre-miR-223	F	ggccaggcctccactcaaggtctcgcttt	expression	this study

StuI			construct cloning	
dre-miR-223 KpnI	R	ggccggtaccgagagtaacaggatcgcatgg	expression construct cloning	this study
dre-*alg2* 3'UTR	F	ccggtacgtagttaggacactgaaggtcatgtgctgtattggtttgaggttgttactgactgtgaatctcctcgtgctattgatattagactgaagacccgaactagtggcc	miR-223 sensor cloning	this study
dre-*alg2* 3'UTR	R	ggccactagttcgggtcttcagtctaatatcaatagcacgaggagattcacagtcagtaacaacctcaaacccaatacagcacatgaccttcagtgtcctaactacgtaccgg	miR-223 sensor cloning	this study
dre-*lman2lb* 3'UTR	F	ccggtacgtacagatatttgtgcgtttttctgtaatttttgtaccaattacactgaccttggcctttctccctgtgacagcatttacagaggctaaagagttcaacgtcaactgtactagtggcc	miR-223 sensor cloning	this study
dre-*lman2lb* 3'UTR	R	ggccactagtacagttgacgttgaactctttagcctctgtaaatgctgtcacagggagaaaggccaaggtcagtgtaattggtacaaaaattacagaaaaacgcacaaatatctgtacgtaccgg	miR-223 sensor cloning	this study
dre-*st3gal2* 3'UTR	F	ccggtacgtagatcattcctctgctctgaggaggagggatagattgatactcaataccagaaactgaaaaccactgacacacagtcactagtggcc	miR-223 sensor cloning	this study
dre-*st3gal2* 3'UTR	R	ggccactagtgactgtgtgtcagtggttttcagtttctggtattgagtatcaatctatccctcctcctcagagcagaggaatgatctacgtaccgg	miR-223 sensor cloning	this study
ERlucT-IRES-Rluc	F	gccaccatgcgaccctcc	Nglyco sensor cloning	this study
ERlucT-IRES-Rluc	R	ttattgttcatttttgagaactcgctc	Nglyco sensor cloning	this study
dre-*alg2* 223MRE gRNA-1	F	taatacgactcactataggaaggtcatgtgctgtattgttttagagctagaa	gRNA PCR	this study
dre-*alg2* 223MRE gRNA-2	F	taatacgactcactataggtctaatatcaatagcacggttttagagctagaa	gRNA PCR	this study
gRNA universal primer	R	aaaagcaccgactcggtgccactttttcaagttgataacggactagccttattttaacttgctatttctagctctaaaac	gRNA PCR	[52]
dre-*alg2* 223MRE	F	cagcgtctcagcttttgtttag	genotyping	this study
dre-*alg2* 223MRE	R	accgttccatctggtcactc	genotyping	this study
dre-miR-223 geno	F	6FAM- ctgctgcaaacctgcattta	genotyping	this study
dre-miR-223 geno	R	gagagtaacaggatcgcatgg	genotyping	[17]

444

445 **References**

446

447 1 Clements, W. K. & Traver, D. Signalling pathways that control vertebrate haematopoietic
448 stem cell specification. *Nat Rev Immunol* **13**, 336-348, doi:10.1038/nri3443 (2013).

449 2 Gritz, E. & Hirschi, K. K. Specification and function of hemogenic endothelium during
450 embryogenesis. *Cell Mol Life Sci* **73**, 1547-1567, doi:10.1007/s00018-016-2134-0 (2016).

451 3 Medvinsky, A., Rybtsov, S. & Taoudi, S. Embryonic origin of the adult hematopoietic
452 system: advances and questions. *Development* **138**, 1017-1031, doi:10.1242/dev.040998
453 (2011).

454 4 Jagannathan-Bogdan, M. & Zon, L. I. Hematopoiesis. *Development* **140**, 2463-2467,
455 doi:10.1242/dev.083147 (2013).

456 5 Kasper, D. M. & Nicoli, S. Epigenetic and Epitranscriptomic Factors Make a Mark on
457 Hematopoietic Stem Cell Development. *Curr Stem Cell Rep* **4**, 22-32 (2018).

458 6 Bertrand, J. Y. *et al.* Haematopoietic stem cells derive directly from aortic endothelium
459 during development. *Nature* **464**, 108-111, doi:10.1038/nature08738 (2010).

460 7 Boisset, J. C. *et al.* In vivo imaging of haematopoietic cells emerging from the mouse
461 aortic endothelium. *Nature* **464**, 116-120, doi:10.1038/nature08764 (2010).

462 8 Kissa, K. & Herbomel, P. Blood stem cells emerge from aortic endothelium by a novel
463 type of cell transition. *Nature* **464**, 112-115, doi:10.1038/nature08761 (2010).

464 9 Stanley, P., Taniguchi, N. & Aebi, M. in *Essentials of Glycobiology* (eds rd *et al.*) 99-
465 111 (2015).

466 10 Moremen, K. W., Tiemeyer, M. & Nairn, A. V. Vertebrate protein glycosylation:
467 diversity, synthesis and function. *Nat Rev Mol Cell Biol* **13**, 448-462,
468 doi:10.1038/nrm3383 (2012).

469 11 Pinho, S. S. & Reis, C. A. Glycosylation in cancer: mechanisms and clinical implications.
470 *Nat Rev Cancer* **15**, 540-555, doi:10.1038/nrc3982 (2015).

471 12 Lanctot, P. M., Gage, F. H. & Varki, A. P. The glycans of stem cells. *Curr Opin Chem*
472 *Biol* **11**, 373-380, doi:10.1016/j.cbpa.2007.05.032 (2007).

473 13 McKinney-Freeman, S. *et al.* The transcriptional landscape of hematopoietic stem cell
474 ontogeny. *Cell Stem Cell* **11**, 701-714, doi:10.1016/j.stem.2012.07.018 (2012).

475 14 Gerri, C., Marass, M., Rossi, A. & Stainier, D. Y. R. Hif-1alpha and Hif-2alpha regulate
476 hemogenic endothelium and hematopoietic stem cell formation in zebrafish. *Blood* **131**,
477 963-973, doi:10.1182/blood-2017-07-797795 (2018).

478 15 Gore, A. V. *et al.* Epigenetic regulation of hematopoiesis by DNA methylation. *Elife* **5**,
479 e11813, doi:10.7554/eLife.11813 (2016).

480 16 North, T. E. *et al.* Hematopoietic stem cell development is dependent on blood flow. *Cell*
481 **137**, 736-748, doi:10.1016/j.cell.2009.04.023 (2009).

482 17 Kasper, D. M. *et al.* MicroRNAs Establish Uniform Traits during the Architecture of
483 Vertebrate Embryos. *Dev Cell* **40**, 552-565 e555, doi:10.1016/j.devcel.2017.02.021
484 (2017).

485 18 Auer, T. O., Duroure, K., Concordet, J. P. & Del Bene, F. CRISPR/Cas9-mediated
486 conversion of eGFP- into Gal4-transgenic lines in zebrafish. *Nat Protoc* **9**, 2823-2840,
487 doi:10.1038/nprot.2014.187 (2014).

488 19 Butko, E. *et al.* Gata2b is a restricted early regulator of hemogenic endothelium in the
489 zebrafish embryo. *Development* **142**, 1050-1061, doi:10.1242/dev.119180 (2015).

490 20 Chen, M. J., Yokomizo, T., Zeigler, B. M., Dzierzak, E. & Speck, N. A. Runx1 is
491 required for the endothelial to haematopoietic cell transition but not thereafter. *Nature*
492 **457**, 887-891, doi:10.1038/nature07619 (2009).

493 21 Wilkinson, R. N. *et al.* Hedgehog and Bmp polarize hematopoietic stem cell emergence
494 in the zebrafish dorsal aorta. *Dev Cell* **16**, 909-916, doi:10.1016/j.devcel.2009.04.014
495 (2009).

496 22 Zhang, Y., Jin, H., Li, L., Qin, F. X. & Wen, Z. cMyb regulates hematopoietic
497 stem/progenitor cell mobilization during zebrafish hematopoiesis. *Blood* **118**, 4093-4101,
498 doi:10.1182/blood-2011-03-342501 (2011).

499 23 Marcelo, K. L. *et al.* Hemogenic endothelial cell specification requires c-Kit, Notch
500 signaling, and p27-mediated cell-cycle control. *Dev Cell* **27**, 504-515,
501 doi:10.1016/j.devcel.2013.11.004 (2013).

502 24 Johnnidis, J. B. *et al.* Regulation of progenitor cell proliferation and granulocyte function
503 by microRNA-223. *Nature* **451**, 1125-1129, doi:10.1038/nature06607 (2008).

504 25 Baek, D. *et al.* The impact of microRNAs on protein output. *Nature* **455**, 64-71,
505 doi:10.1038/nature07242 (2008).

506 26 Bartel, D. P. Metazoan MicroRNAs. *Cell* **173**, 20-51, doi:10.1016/j.cell.2018.03.006
507 (2018).

508 27 Huffaker, T. C. & Robbins, P. W. Yeast mutants deficient in protein glycosylation. *Proc*
509 *Natl Acad Sci U S A* **80**, 7466-7470 (1983).

510 28 Kamiya, Y. *et al.* Molecular basis of sugar recognition by the human L-type lectins
511 ERGIC-53, VIPL, and VIP36. *J Biol Chem* **283**, 1857-1861,
512 doi:10.1074/jbc.M709384200 (2008).

513 29 Gomez-Navarro, N. & Miller, E. Protein sorting at the ER-Golgi interface. *J Cell Biol*
514 **215**, 769-778, doi:10.1083/jcb.201610031 (2016).

515 30 Hemmoranta, H. *et al.* N-glycan structures and associated gene expression reflect the
516 characteristic N-glycosylation pattern of human hematopoietic stem and progenitor cells.
517 *Exp Hematol* **35**, 1279-1292, doi:10.1016/j.exphem.2007.05.006 (2007).

518 31 Sturgill, E. R. *et al.* Biosynthesis of the major brain gangliosides GD1a and GT1b.
519 *Glycobiology* **22**, 1289-1301, doi:10.1093/glycob/cws103 (2012).

520 32 Giordanengo, V. *et al.* Cloning and expression of cDNA for a human Gal(beta1-
521 3)GalNAc alpha2,3-sialyltransferase from the CEM T-cell line. *Eur J Biochem* **247**, 558-
522 566 (1997).

523 33 Nicoli, S. *et al.* MicroRNA-mediated integration of haemodynamics and Vegf signalling
524 during angiogenesis. *Nature* **464**, 1196-1200, doi:10.1038/nature08889 (2010).

525 34 Murayama, E. *et al.* Tracing hematopoietic precursor migration to successive
526 hematopoietic organs during zebrafish development. *Immunity* **25**, 963-975,
527 doi:10.1016/j.immuni.2006.10.015 (2006).

528 35 Contessa, J. N. *et al.* Molecular imaging of N-linked glycosylation suggests glycan
529 biosynthesis is a novel target for cancer therapy. *Clin Cancer Res* **16**, 3205-3214,
530 doi:10.1158/1078-0432.CCR-09-3331 (2010).

531 36 DeRossi, C. *et al.* trappc11 is required for protein glycosylation in zebrafish and humans.
532 *Mol Biol Cell* **27**, 1220-1234, doi:10.1091/mbc.E15-08-0557 (2016).

533 37 Esko, J. D., Bertozzi, C. & Schnaar, R. L. in *Essentials of Glycobiology* (eds rd *et al.*)
534 701-712 (2015).

535 38 Pilobello, K. T., Slawek, D. E. & Mahal, L. K. A ratiometric lectin microarray approach
536 to analysis of the dynamic mammalian glycome. *Proc Natl Acad Sci U S A* **104**, 11534-
537 11539, doi:10.1073/pnas.0704954104 (2007).

538 39 Pilobello, K. T., Agrawal, P., Rouse, R. & Mahal, L. K. Advances in lectin microarray
539 technology: optimized protocols for piezoelectric print conditions. *Curr Protoc Chem*
540 *Biol* **5**, 1-23, doi:10.1002/9780470559277.ch120035 (2013).

541 40 Wang, L., Liu, Y., Wu, L. & Sun, X. L. Sialyltransferase inhibition and recent advances.
542 *Biochim Biophys Acta* **1864**, 143-153, doi:10.1016/j.bbapap.2015.07.007 (2016).

543 41 Perlin, J. R., Robertson, A. L. & Zon, L. I. Efforts to enhance blood stem cell
544 engraftment: Recent insights from zebrafish hematopoiesis. *J Exp Med* **214**, 2817-2827,
545 doi:10.1084/jem.20171069 (2017).

546 42 Rowe, R. G., Mandelbaum, J., Zon, L. I. & Daley, G. Q. Engineering Hematopoietic
547 Stem Cells: Lessons from Development. *Cell Stem Cell* **18**, 707-720,
548 doi:10.1016/j.stem.2016.05.016 (2016).

549 43 Sminia, T. J., Zuilhof, H. & Wennekes, T. Getting a grip on glycans: A current overview
550 of the metabolic oligosaccharide engineering toolbox. *Carbohydr Res* **435**, 121-141,
551 doi:10.1016/j.carres.2016.09.007 (2016).

552 44 Zhang, P. *et al.* Challenges of glycosylation analysis and control: an integrated approach
553 to producing optimal and consistent therapeutic drugs. *Drug Discov Today* **21**, 740-765,
554 doi:10.1016/j.drudis.2016.01.006 (2016).

555 45 Boheler, K. R. & Gundry, R. L. Concise Review: Cell Surface N-Linked Glycoproteins
556 as Potential Stem Cell Markers and Drug Targets. *Stem Cells Transl Med* **6**, 131-138,
557 doi:10.5966/sctm.2016-0109 (2017).

558 46 Choi, J. *et al.* FoxH1 negatively modulates flk1 gene expression and vascular formation
559 in zebrafish. *Dev Biol* **304**, 735-744, doi:10.1016/j.ydbio.2007.01.023 (2007).

560 47 Asakawa, K. *et al.* Genetic dissection of neural circuits by Tol2 transposon-mediated
561 Gal4 gene and enhancer trapping in zebrafish. *Proc Natl Acad Sci U S A* **105**, 1255-1260,
562 doi:10.1073/pnas.0704963105 (2008).

563 48 Distel, M., Wullimann, M. F. & Koster, R. W. Optimized Gal4 genetics for permanent
564 gene expression mapping in zebrafish. *Proc Natl Acad Sci U S A* **106**, 13365-13370,
565 doi:10.1073/pnas.0903060106 (2009).

566 49 Auer, T. O., Duroure, K., De Cian, A., Concordet, J. P. & Del Bene, F. Highly efficient
567 CRISPR/Cas9-mediated knock-in in zebrafish by homology-independent DNA repair.
568 *Genome Res* **24**, 142-153, doi:10.1101/gr.161638.113 (2014).

569 50 Moreno-Mateos, M. A. *et al.* CRISPRscan: designing highly efficient sgRNAs for
570 CRISPR-Cas9 targeting in vivo. *Nat Methods* **12**, 982-988, doi:10.1038/nmeth.3543
571 (2015).

572 51 Vejnar, C. E., Moreno-Mateos, M. A., Cifuentes, D., Bazzini, A. A. & Giraldez, A. J.
573 Optimized CRISPR-Cas9 System for Genome Editing in Zebrafish. *Cold Spring Harb*
574 *Protoc* **2016**, doi:10.1101/pdb.prot086850 (2016).

575 52 Narayanan, A. *et al.* In vivo mutagenesis of miRNA gene families using a scalable
576 multiplexed CRISPR/Cas9 nuclease system. *Sci Rep* **6**, 32386, doi:10.1038/srep32386
577 (2016).

578 53 Ristori, E. & Nicoli, S. miRNAs expression profile in zebrafish developing vessels.
579 *Methods Mol Biol* **1214**, 129-150, doi:10.1007/978-1-4939-1462-3_7 (2015).

580 54 Burns, C. E., Traver, D., Mayhall, E., Shepard, J. L. & Zon, L. I. Hematopoietic stem cell
581 fate is established by the Notch-Runx pathway. *Genes Dev* **19**, 2331-2342,
582 doi:10.1101/gad.1337005 (2005).

583 55 Thompson, M. A. *et al.* The cloche and spadetail genes differentially affect
584 hematopoiesis and vasculogenesis. *Dev Biol* **197**, 248-269, doi:10.1006/dbio.1998.8887
585 (1998).

586 56 Fang, J. S., Gritz, E. C., Marcelo, K. L. & Hirschi, K. K. Isolation of Murine Embryonic
587 Hemogenic Endothelial Cells. *J Vis Exp*, doi:10.3791/54150 (2016).

588 57 Villefranc, J. A., Amigo, J. & Lawson, N. D. Gateway compatible vectors for analysis of
589 gene function in the zebrafish. *Dev Dyn* **236**, 3077-3087, doi:10.1002/dvdy.21354 (2007).

590 58 Kwan, K. M. *et al.* The Tol2kit: a multisite gateway-based construction kit for Tol2
591 transposon transgenesis constructs. *Dev Dyn* **236**, 3088-3099, doi:10.1002/dvdy.21343
592 (2007).

593 59 Bensing, B. A., Li, Q., Park, D., Lebrilla, C. B. & Sullam, P. M. Streptococcal Siglec-like
594 adhesins recognize different subsets of human plasma glycoproteins: implications for
595 infective endocarditis. *Glycobiology* **28**, 601-611, doi:10.1093/glycob/cwy052 (2018).

596 60 Link, V., Shevchenko, A. & Heisenberg, C. P. Proteomics of early zebrafish embryos.
597 *BMC Dev Biol* **6**, 1, doi:10.1186/1471-213X-6-1 (2006).
598
599

Author Contributions

D.M.K. and S.N. designed and conducted experiments, analyzed data, and wrote the manuscript. H.K.M, K.S., J.G., J.H., and W.A. carried out zebrafish experiments and analyzed data. K.K.H., Y.W. and Z.H. designed and performed mouse phenotypic experiments and analyses. L.K.M. and D.W.H. conducted lectin microarray analysis. W.C.S. and EJ. P. created and shared the N-glycosensor. All authors edited the paper.

Acknowledgments

The authors would like to thank Meredith Cavanaugh for fish husbandry and care. We would also like to acknowledge Angela Anderson, Valentina Greco, Daniel DiMaio, Liana C. Boraas, and Siyuan Chen for critical reading of the manuscript. This work was supported by grants from the NIH (R01HL130246 and R56DK118728 to S.N. and F32HL132475, U54DK106857, and 1K99HL141687 to D.K.

Competing interests

The authors declare no competing interests.

Corresponding authors

Correspondence to Stefania Nicoli and Karen K. Hirschi.

620 **Figure 1**

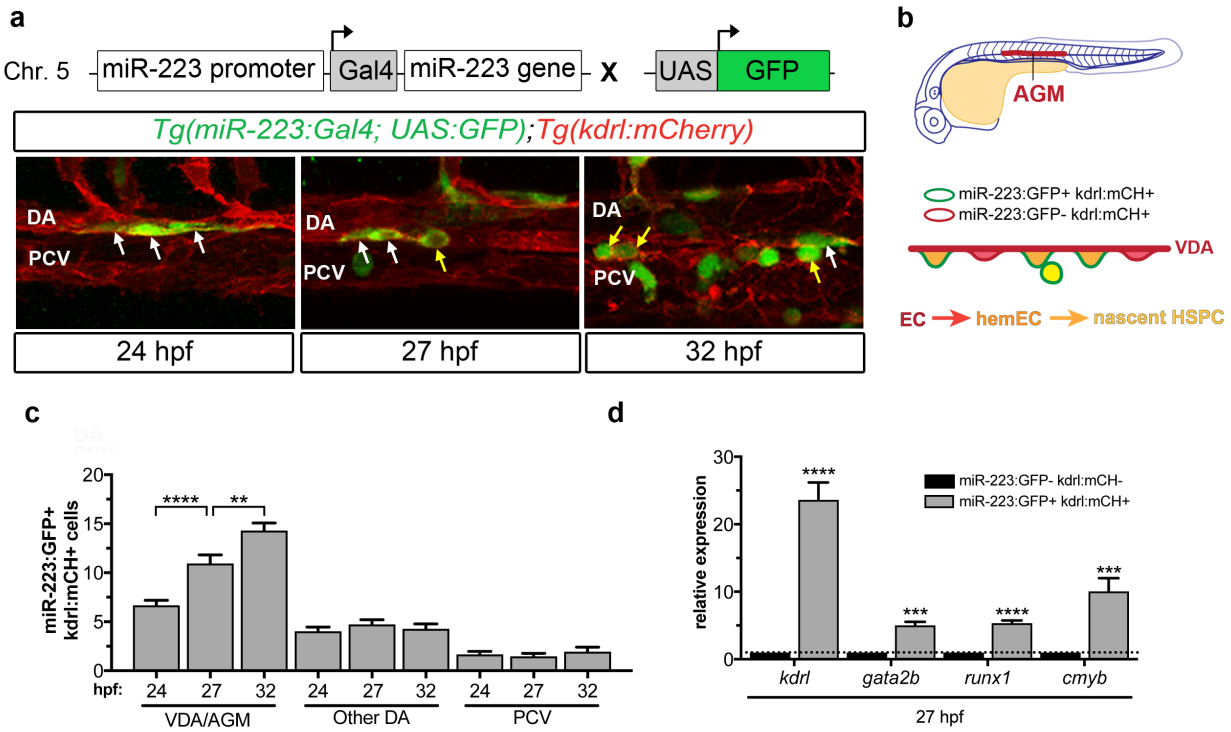

621
622 **Figure 1. miR-223 is expressed in hemogenic endothelial cells undergoing EHT**
623 **a,** *top,* Schematic of miR-223:Gal4 reporter integrated into the endogenous miR-223 locus. Gal4
624 activates UAS:GFP to fluorescently mark miR-223-expressing cells (miR-223:GFP+). *bottom,*
625 Lateral maximum confocal projections of the zebrafish AGM. White and yellow arrows point to
626 flat and budding miR-223:GFP+; kdrl:mCH+ endothelial cells in the VDA, respectively. **b,**
627 Overview of zebrafish EHT. In the AGM region, flattened endothelial cells (red) gain hemogenic
628 potential (orange), round up, and bud as nascent HSPCs (yellow) from the VDA wall into the
629 PCV circulation from 24-48 hpf. Cells outlined in green or red represent miR-223:GFP+
630 kdrl:mCH+ or miR-223:GFP- kdrl:mCH+ endothelial cells, respectively. **c,** Mean ± SEM
631 number of miR-223:GFP+; kdrl:mCH+ endothelial cells in the VDA of the AGM compared to
632 other regions in the DA and in the PCV (n = 36-43 embryos). Significance determined by
633 unpaired, two-tailed Mann-Whitney U test. **d,** Mean ± SEM fold change expression in miR-
634 223:GFP+ kdrl:mCH+ endothelial cells relative to miR-223:GFP- kdrl:mCH- non-endothelial
635 cells at 27 hpf by qRT-PCR (n = 3 technical replicates). Significance determined by a paired,
636 two-tailed, Student's t-test. For all plots, significance calculations are represented as $^{**}p \leq$
637 0.01, $^{***}p \leq 0.01$, $^{****}p \leq 0.0001$ Abbreviations: AGM, aorta-gonad mesonephros; DA, dorsal
638 aorta; EC, endothelial cell; EHT, endothelial-to-hematopoietic transition; hemEC, hemogenic
639 endothelial cell, HSPC, hematopoietic stem/progenitor cell; PCV, posterior cardinal vein; VDA,
640 ventral dorsal aorta
641
642

643 **Figure 2.**

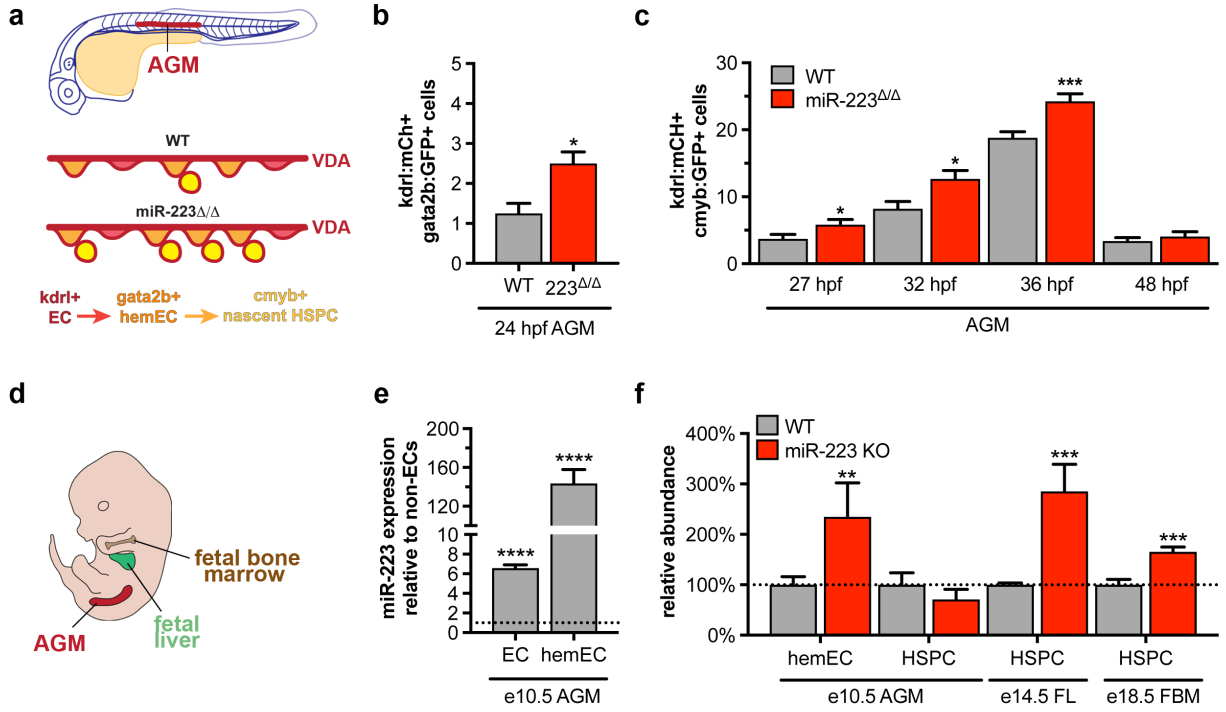

644
645 **Figure 2. miR-223 is a conserved endothelial inhibitor of EHT and HSPC production**
646 **a,** Schematic illustrates the EHT defects observed in the zebrafish miR-223Δ/Δ VDA of the
647 AGM compared to wild-type. Cell types involved in EHT are color-coded according to their
648 defining markers. **b,** Mean ± SEM number of kdrl:mCH+ gata2b:GFP+ cells in the VDA of the
649 zebrafish AGM during EHT (n = 4 embryos). **c,** Mean ± SEM number of kdrl:mCH+
650 cmyb:GFP+ cells in the VDA of the zebrafish AGM during EHT (n = 14-36 embryos). 36 hpf
651 data was previously published[17] and re-plotted for reference. **d**, Schematic depicts mouse
652 embryonic hematopoietic sites. HSPCs are produced in the AGM and mature as they transit to
653 the fetal liver, and then fetal bone marrow. **e,** Mean ± SEM fold change of mature miR-223
654 expression in wild-type FAC-sorted mouse endothelial cells (CD31+CD45-SP-) and hemECs
655 (Flk1+cKit+CD45- SP+) relative to non-endothelial cells (CD31-CD45-) in the e10.5 AGM (n =
656 3 technical replicates). **f,** Mean ± SEM percentage of hemECs (Flk+cKit+CD45- SP+) (n = 6
657 replicates) or HSPCs (cKit+Sca+ Lin-) at indicated hematopoietic sites at e10.5 (n = 5-8
658 replicates), e14.5 (n = 16 replicates), and e18.5 (n = 7 replicates) in the miR-223KO relative to
659 wild-type. For all plots, significance calculations are represented as $^{*}p \leq 0.05$, $^{**}p \leq 0.01$, $^{***}p \leq$
660 0.01, $^{****}p \leq 0.0001$, two-tailed Student's t-test. Abbreviations: AGM, aorta-gonad mesonephros;
661 EC, endothelial cell; EHT, endothelial-to-hematopoietic transition; FBM, fetal bone marrow,
662 FBM; FL, fetal liver; hemEC, hemogenic endothelial cells, HSPC, hematopoietic
663 stem/progenitor cell; PCV, posterior cardinal vein; VDA, ventral dorsal aorta
664
665

666 **Figure 3.**

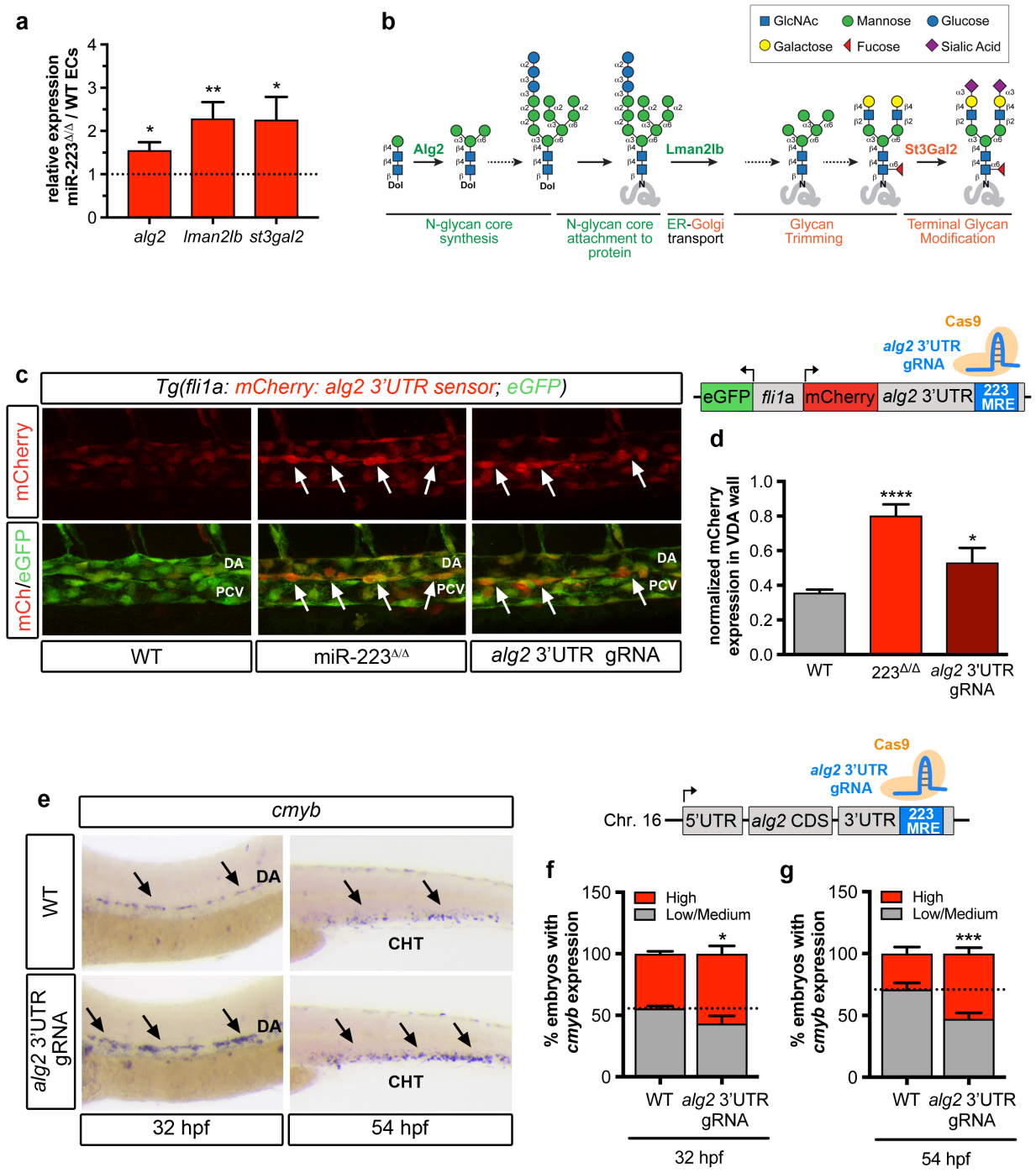

667
668 *Figure 3. Legend (next page)*
669

670 **Figure 3. miR-223 targets N-glycogenes to limit HSPC production**
671 **a,** Mean ± SEM fold change expression of N-glycogenes putatively targeted by miR-223 in
672 miR-223Δ/Δ relative to wild-type kdrl:GFP+ endothelial cells at 27 hpf by qRT-PCR (n = 6-7
673 biological replicates). **b,** Schematic shows the biosynthesis of a hypothetical N-glycan (also see
674 text and Supplementary Fig. 3a). Solid and dotted arrows indicate single and multiple steps
675 occurring during the process, respectively. Only N-glycogenes putatively targeted by miR-223
676 are indicated and are color-coded based on their function in the ER (green) or Golgi (orange)
677 during N-glycosylation. **c,** Lateral confocal Z-projections of the stable *Tg(fli1a:mCherry-alg2*
678 *3'UTR sensor: eGFP)* transgenic line in the zebrafish AGM at 32 hpf. Arrows indicate mCherry
679 de-repression in endothelial cells along the VDA wall of embryos deficient for miR-223 or
680 injected with Cas9 mRNA and a gRNA that disrupts miR-223 binding to the *alg2* 3'UTR-miR-
681 223 MRE sensor. **d,** Mean ± SEM mCherry intensity normalized to eGFP along the length of the
682 VDA wall in the AGM of 32 hpf embryos stably expressing *alg2* 3'UTR-miR-223 MRE sensor
683 (n = 8-11 embryos) **e,** Representative expression of HSPC marker *cmyb* in the AGM at 32 hpf or
684 CHT at 54 hpf (arrows) of zebrafish embryos injected with a gRNA that disrupts miR-223
685 binding to the endogenous *alg2* 3'UTR by whole mount in situ hybridization. **f, g** Mean ± SEM
686 percentage of embryos with high or low/medium *cmyb* expression in the 32 hpf DA (**f**) or 54 hpf
687 CHT (**g**) (n = 3 biological replicates). For all plots, significance calculations are represented as $^{*}p$
688 ≤ 0.05, $^{**}p \leq 0.01$, $^{***}p \leq 0.01$, $^{****}p \leq 0.0001$, two-tailed Student's t-test. Abbreviations: AGM,
689 aorta-gonad mesonephros; DA, dorsal aorta; Dol, dolichol lipid; CHT, caudal hematopoietic
690 tissue, GlcNAc, N-acetylglucosamine; gRNA, guide RNA; HSPC, hematopoietic
691 stem/progenitor cell; MRE, miRNA responsive element; PCV, posterior cardinal vein; ER,
692 endoplasmic reticulum; VDA, ventral dorsal aorta
693
694

695 **Figure 4.**

696

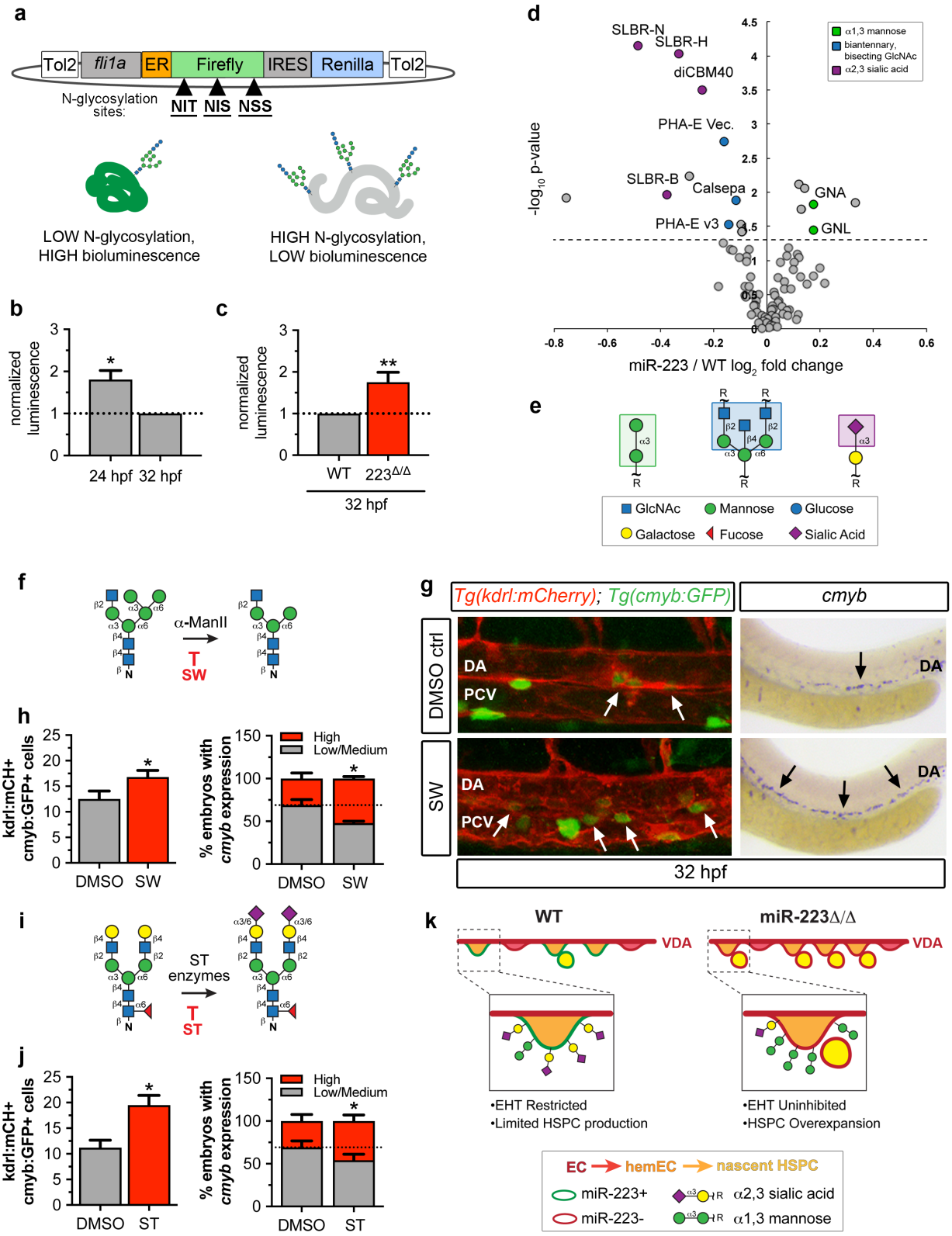

697

698 *Figure 4 legend (next page)*

Figure 4. miR-223 regulates the endothelial N-glycome during EHT.
a, Design of the N-glycosensor construct. The endothelial *fli1a* promoter drives co-expression of firefly luciferase, tagged with an ER translation sequence, and an un-localized renilla luciferase normalization control. Firefly luciferase localization to the ER permits glycosylation of its three naturally occurring N-glycosylation consensus sites, consisting of asparagine-X-serine/threonine (N-X-S/T), where X is any amino acid except proline. Firefly bioluminescence is affected by the extent of ectopic glycan addition as indicated. **b,** Mean ± SEM firefly normalized to renilla bioluminescence in wild-type endothelial cells at 24 hpf relative to 32 hpf. **c,** Mean ± SEM firefly normalized to renilla bioluminescence in miR-223Δ/Δ relative to wild-type endothelial cells at 32 hpf. **d,** Volcano plot depicts $\log_2$ fold change of glycans in 32 hpf miR-223Δ/Δ (n = 8 biological replicates) relative to wild-type (n = 5 biological replicates) by ratiometric lectin microarray. Dots represent discrete glycan moieties recognized by individual lectins. Glycan types that were significantly changed and recognized by multiple lectins are indicated, including α1,3 mannose (green), biantennary N-glycan stuctures with bisecting GlcNAc (blue), and α2,3 sialic acid (purple). Dotted treadline indicates a significant $-\log_{10}(0.05)$ p-value. **e,** Structures for N-glycans highlighted in **d**. Shaded boxes indicate binding specificities of associated lectins and are color coded accordingly. **f, i,** N-glycan structures depict the inhibitory activities of SW and ST. SW is an α-Mannosidase II inhibitor that removes the α1,3 and α1,6 mannoses indicated in the diagram (**f**). ST is a pan-sialyltransferase inhibitor that prevents terminal sialic acid modification (**i**). **g,** Representative images depict the zebrafish AGM at 32 hpf upon treatment with 5 μg/ml SW compared to 0.2% DMSO control from 8-32 hpf. White arrows in confocal projections (*left*) point to representative kdrl:mCh+ cmyb:gfp+ cells undergoing EHT in the VDA. Black arrows in bright field images (*right*) show *cmyb* expression in the AGM by whole mount in situ hybridization. **h, j,** Mean ± SEM number of kdrl:mCh+ cmyb:gfp+ cells in the VDA of embryos treated with SW (**h,** *left*) or ST (**j,** *left*) compared to the respective DMSO control at 32 hpf (n = 10 embryos). Mean ± SEM percentage of embryos with high or low/medium *cmyb* expression upon treatment with SW (**h,** *right*) (n = 4 biological replicates) or ST (**j,** *right*) compared to the respective DMSO control (n = 5 biological replicates). **k,** Model illustrates how miR-223-dependent regulation of the endothelial N-glycome restricts EHT and HSPC production. α1,3 mannose and α2,3 sialic acid glycans on membrane proteins are altered upon loss of miR-223 activity as shown. This altered "sugar code" promotes hemEC transition to HSPCs. miR-223+ expressing and non-expressing cells are outlined in green and red, respectively. Only relevant N-glycan moieties are depicted. For all plots, significance calculations are represented as $^{*}p \leq 0.05$, $^{**}p \leq 0.01$, two-tailed Student's t-test. Abbreviations: AGM, aorta-gonad mesonephros; DA, dorsal aorta; EHT, endothelial-to-hematopoietic transition; ER, endoplasmic reticulum; GlcNAc, N-acetylglucosamine; HSPC, hematopoietic stem/progenitor cell; IRES, internal ribosome entry site; PCV, posterior cardinal vein; ST, sialyltransferase inhibitor; SW, swainosine; VDA, ventral dorsal aorta

742 **Supplementary Figure 1.**

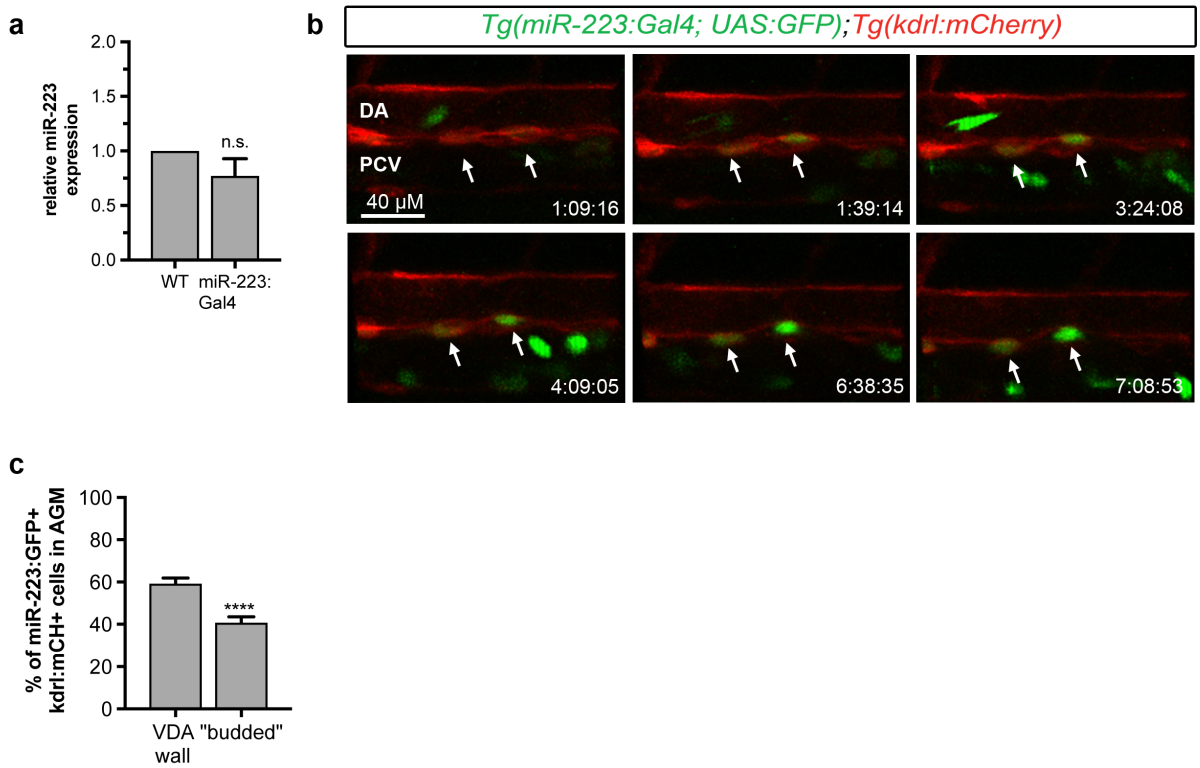

743
744 **Supplementary Figure 1. miR-223-expressing cells delaminate from AGM**
745 **a,** Mean ± SEM fold change of mature miR-223 expression in *Tg(miR-223:Gal4)*$^{ya362/+}$ relative
746 to non-transgenic wild-type embryos at 32 hpf by qRT-PCR (n = 4 biological replicates). **b,**
747 Lateral maximum confocal Z-projection of time-lapse movie frames during EHT. Arrows point
748 to two miR-223:GFP+; kdrl:mCH+ cells budding from the VDA in the AGM. Relative time is
749 indicated in hr:min:sec (see also Supplementary Movie 1). **c,** Mean ± SEM percentage of miR-
750 223:GFP+ kdrl:mCH+ endothelial cells/ embryo that are within the VDA wall or appear to have
751 "budded" from the VDA into the sub-aortic space between the DA and PCV at 32 hpf (n = 36
752 embryos). For all plots, significance calculations are represented as n.s. (not significant, $p > 0.05$),
753 $^{****}p \leq 0.0001$, two-tailed Student's t-test. Abbreviations: AGM, aorta-gonad mesonephros; DA,
754 dorsal aorta; hemEC, hemogenic endothelial cells, PCV, posterior cardinal vein; VDA, ventral
755 dorsal aorta
756
757

758 **Supplementary Figure 2.**

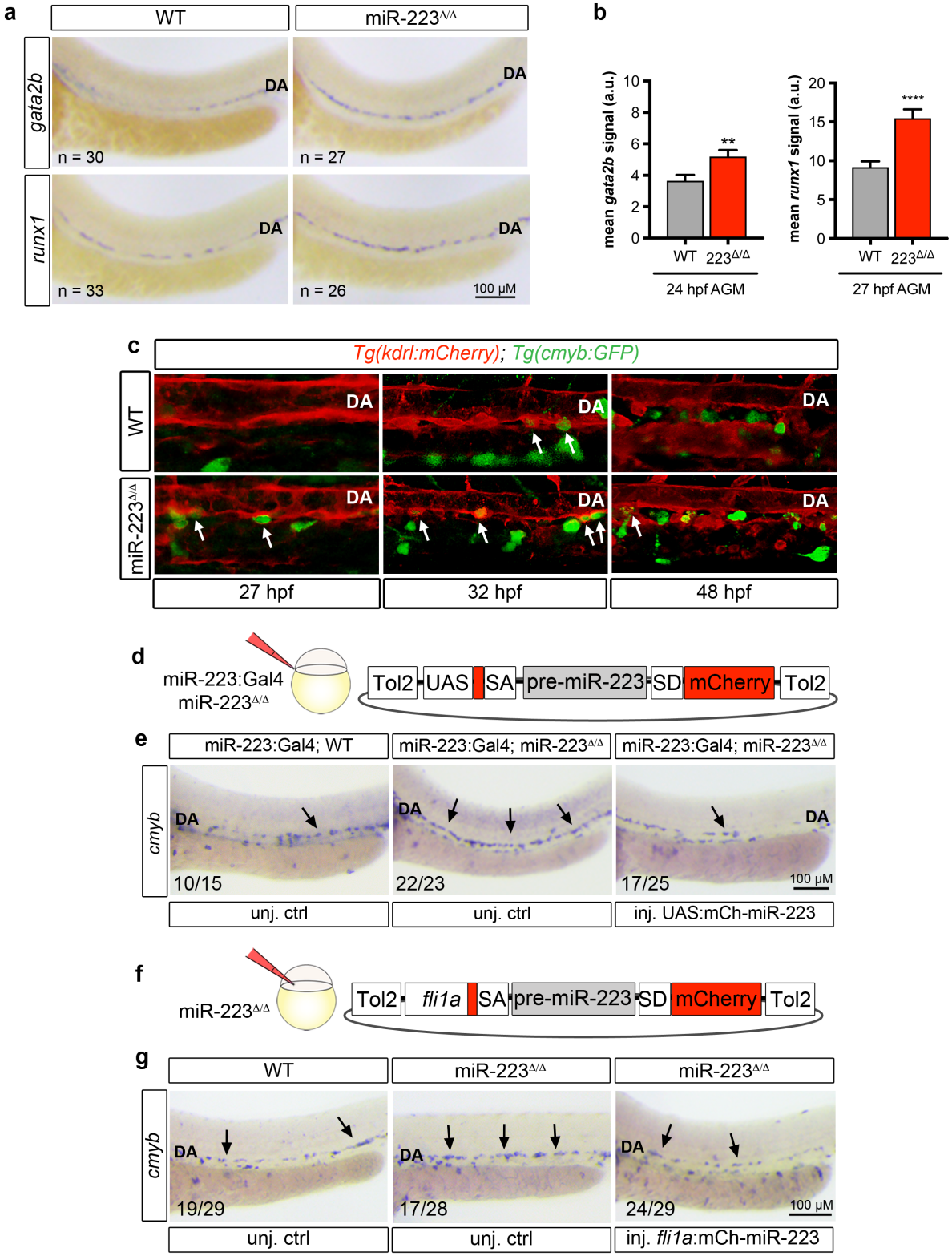

759
760
761 *Supplementary Figure 2 Legend (next page)*

Supplementary Figure 2. miR-223 restricts EHT and HSPC production.
a, Representative expression of *gata2b* (*top*) and *runx1* (*bottom*) in the wild-type or miR-223Δ/Δ AGM by WISH. **b,** Quantification of *gata2b* (*left*) and *runx1* (*right*) WISH staining in **a.** Bar plots show normalized mean WISH signal ± SEM (n values are indicated in **a**). **c,** Representative confocal projections for Fig. 2c quantification. Arrows point to representative examples of kdrl:mCH+ cmyb:GFP+ cells undergoing EHT from the VDA in the zebrafish AGM. **d,** Schematic of *Tg(UAS:mCherry-miR-223)* construct to re-express miR-223 using miR-223:Gal4+ line via Tol2-mediated transgenesis. A UAS promoter drives expression of the pre-miR-223 precursor within an intron of mCherry. Splicing of this transcript liberates the pre-miR-223 stem loop, allowing it to be further processed into its mature and active form. **e,** Images show representative *cmyb* expression in the AGM (arrows) of miR-223:Gal4; miR-223Δ/Δ embryos injected with *Tg(UAS:mCherry-miR-223)* in **d** and uninjected controls at 32 hpf by WISH. Re-introduction of miR-223 into miR-223:Gal4+ cells rescues miR-223Δ/Δ *cmyb*+ HSPC overexpansion. **f,** Construct as in **d**, except the endothelial *fli1a* enhancer/promoter drives miR-223 expression. **g,** Images show representative *cmyb* expression in the AGM (arrows) of miR-223Δ/Δ embryos injected with *Tg(fli1a ep:mCherry-miR-223)* in **f** and uninjected controls at 32 hpf by WISH. Re-introduction of miR-223 into endothelial cells rescues miR-223Δ/Δ *cmyb*+ HSPC overexpansion. For all plots, significance calculations are represented as $^{**}p \leq 0.01$, $^{****}p \leq 0.0001$, unpaired two-tailed Student's t-test. Abbreviations: AGM, aorta-gonad mesonephros; DA, dorsal aorta; EHT, endothelial-to-hematopoietic transition; HSPC, hematopoietic stem/progenitor cell; inj, injected; unj, uninjected; SA, splice acceptor site; SD, splice donor site; VDA, ventral dorsal aorta; WISH, whole mount in situ hybridization.

786 **Supplementary Figure 3.**
787

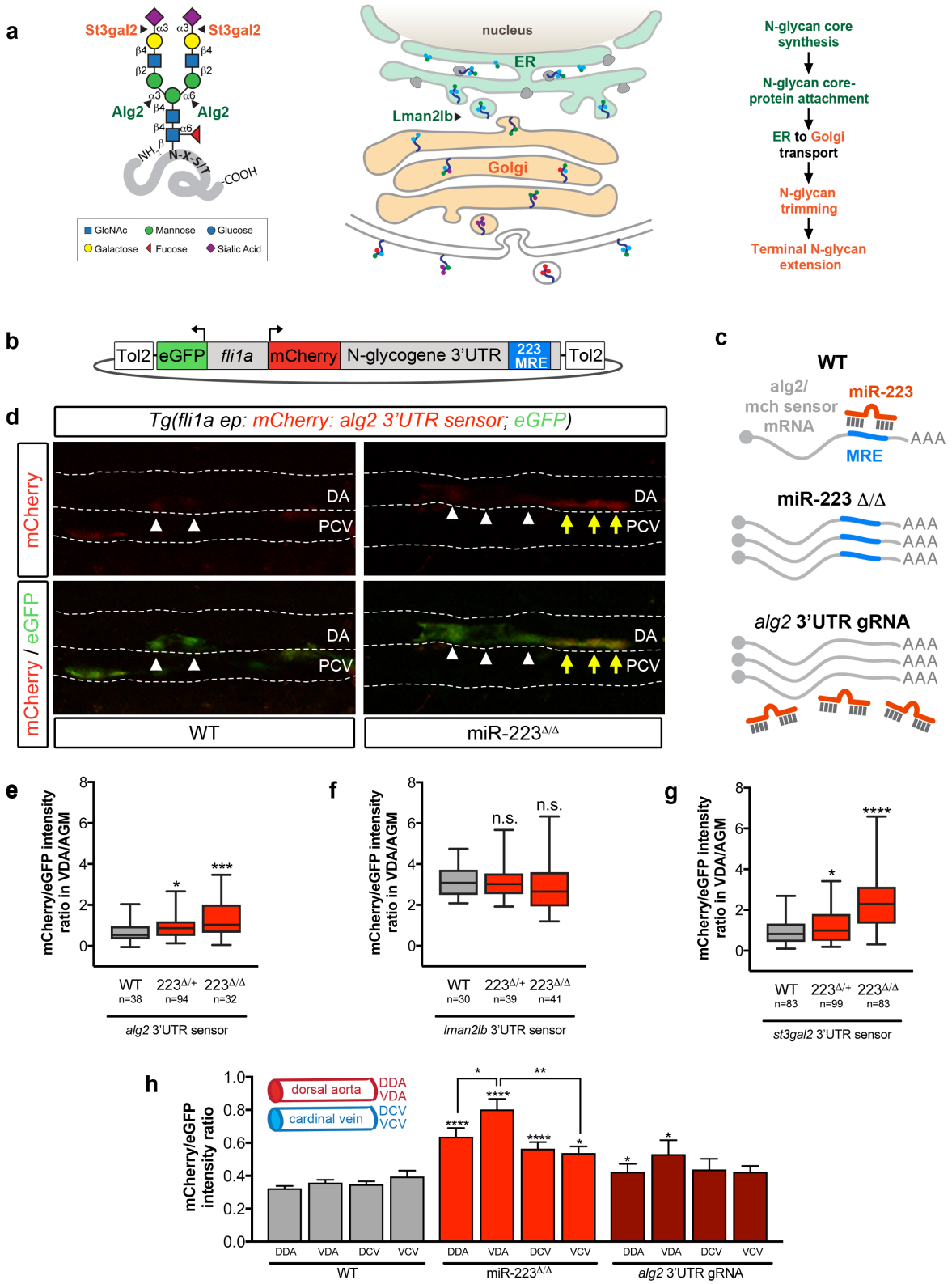

788
789 *Supplementary Figure 3 Legend (next page)*

Supplementary Figure 3. miR-223 targets N-glycosylation genes in the AGM during EHT. **a,** Overview of N-glycan biosynthesis. Putative miR-223 target genes are indicated and color-coded based on their function in the ER (green) or Golgi (orange) during N-glycosylation. Black arrowheads point to Alg2 and St3Gal2 glycosyltransferase activities on a hypothetical N-glycan core after its addition to a polypeptide chain, and to the ER-Golgi transport function of Lman2lb. (See also text and Fig. 3b). **b,** Endothelial N-glycogene-3'UTR-miR-223 MRE sensor construct to test direct miR-223 targeting of N-glycogenes. The *fli1a* enhancer/promoter drives co-expression of mCherry controlled by a ~100-125 bp N-glycogene 3'UTR fragment containing the miR-223 MRE, and an unregulated eGFP normalization control. **c,** Schematic illustrates de-repression of endogenous *alg2* or N-glycogene sensor mRNAs upon loss of miR-223 activity. **d,** Representative confocal micrographs showing Tol2-mediated mosaic integration of the *alg2* 3'UTR-miR-223 MRE sensor at 32 hpf in the zebrafish AGM. White arrowheads point to mCherry repression in endothelial cells along the VDA wall. Upon miR-223 depletion, mCherry is de-repressed in a subset of these cells (yellow arrows), consistent with the salt and pepper miR-223 expression pattern (See Fig. 1a). **e-g,** Box-plots show mCherry intensity normalized to eGFP for AGM endothelial cells in 32 hpf embryos mosaically-expressing the *alg2* (**e**), *lman2lb* (**f**), or *st3gal2* (**g**) 3'UTR-miR-223 MRE sensors. Embryos were derived from miR-223Δ/+ in-crosses. n values are indicated and represent the number of endothelial cells analyzed. Significance was determined by two-tailed Mann-Whitney U test. **h,** Mean ± SEM mCherry intensity normalized to eGFP along the length of the axial vessel walls in the AGM of 32 hpf embryos stably-expressing the *alg2* 3'UTR-miR-223 MRE sensor. Axial vessel walls include the dorsal (D) and ventral (V) walls of the DA (red) or PCV (blue), referred to as DDA, VDA, DCV, and VCV, respectively, as depicted in the graph schematic (n = 8-11 embryos, two-tailed Student's t-test.) For all plots, significance calculations are represented as n.s. (not significant, $p > 0.05$), $^{*}p \leq 0.05$, $^{**}p \leq 0.01$, $^{***}p \leq 0.001$, $^{****}p \leq 0.0001$. Abbreviations: AGM, aorta-gonad mesonephros; DA, dorsal aorta; ER, endopasmic reticulum; GlcNAc, N-acetylglucosamine; gRNA, guide RNA; MRE, miRNA responsive element; PCV, posterior cardinal vein

819 **Supplementary Figure 4.**

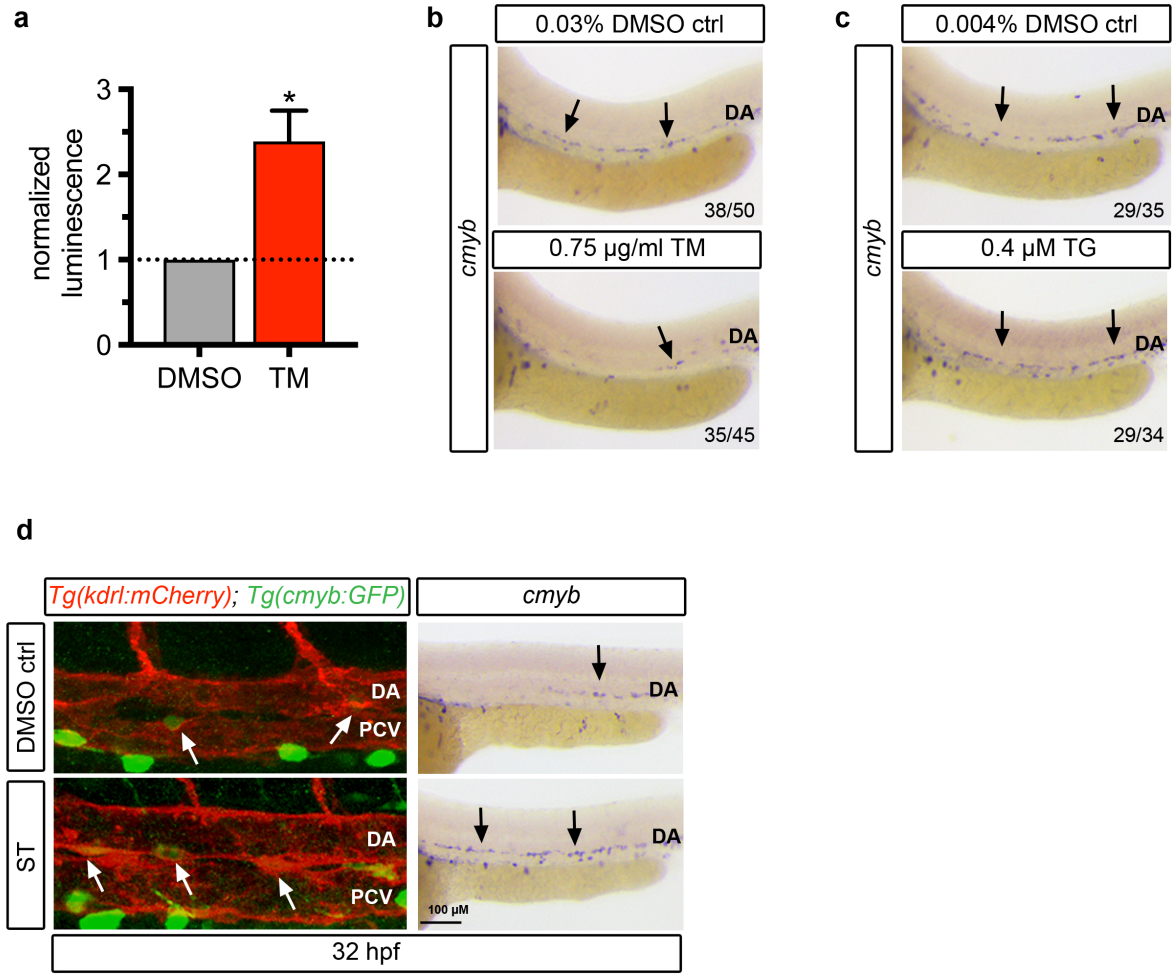

820
821 **Supplementary Figure 4. Hypoglycosylation and ER-stress do not lead to HSPC**
822 **overexpansion.**
823 **a,** Mean ± SEM firefly normalized to renilla bioluminescence in endothelial cells of wild-type
824 embryos injected with the N-glycosensor (see Fig. 3a) and treated with TM relative to DMSO
825 control (n = 6 biological replicates) at 32 hpf (n = 6 biological replicates). Significance is
826 represented as $^{*}p \leq 0.05$, paired, two-tailed Student's t-test. **b, c** Images show representative *cmyb*
827 expression in the AGM (arrows) of 32 hpf wild-type embryos treated with TM (**b**), TG (**c**), and
828 the respective DMSO control by WISH. **d,** Representative images depict the zebrafish AGM at
829 32 hpf upon treatment with 200 µg/ml ST compared to 2% DMSO control from 8-32 hpf. White
830 arrows in confocal projections (*left*) point to representative kdrl:mCh+ cmyb:gfp+ cells
831 undergoing EHT in the VDA. Black arrows in bright field images (*right*) show representative
832 *cmyb* expression in the AGM by WISH. Abbreviations: AGM, aorta-gonad mesonephros; DA,
833 dorsal aorta; PCV, posterior cardinal vein; TG, thapsigargin; TM, tunicamycin; VDA, ventral
834 dorsal aorta; WISH, whole mount in situ hybridization
835

836 **Supplementary Movie 1. miR-223-expressing cells delaminate from AGM**
837 Lateral maximum confocal Z-projection of a time-lapse movie during EHT. Two miR-
838 223:GFP+; kdrl:mCH+ cells are shown budding from the ventral dorsal aorta in the AGM.
839 Relative time is indicated in hr:min:sec (see also Supplementary Fig. 1b).